

Detection of cesium in the atmosphere of the hot He-rich white dwarf HD 149499B

P. Chayer,¹[★] C. Mendoza,² M. Meléndez,¹ J. Deprince^{3,4} and J. Dupuis⁵

¹Space Telescope Science Institute, 3700 San Martin Drive, Baltimore, MD 21218, USA

²Physics Center, Venezuelan Institute for Scientific Research (IVIC), Caracas 1020, Venezuela

³Cahill Center for Astronomy and Astrophysics, California Institute of Technology, Pasadena, CA 91125, USA

⁴Physique Atomique et Astrophysique, Université de Mons – UMONS, 7000 Mons, Belgium

⁵Canadian Space Agency, 6767 Route de l'Aéroport, Saint-Hubert, QC J3Y 8Y9, Canada

Accepted 2022 October 26. Received 2022 September 26; in original form ZZZ

ABSTRACT

We report the first detection of cesium ($Z = 55$) in the atmosphere of a white dwarf. Around a dozen absorption lines of Cs IV, Cs V, and Cs VI have been identified in the *Far Ultraviolet Spectroscopic Explorer* spectrum of the He-rich white dwarf HD 149499B ($T_{\text{eff}} = 49,500$ K, $\log g = 7.97$). The lines have equivalent widths ranging from 2.3 to 26.9 mÅ. We performed a spectral synthesis analysis to determine the cesium content in the atmosphere. Non-LTE atmosphere models were computed by considering cesium explicitly in the calculations. For this purpose we calculated oscillator strengths for the bound–bound transitions of Cs IV–Cs VI with both AUTOSTRUCTURE (multiconfiguration Breit–Pauli) and GRASP2K (multiconfiguration Dirac–Fock) atomic structure codes as neither measured nor theoretical values are reported in the literature. We determined a cesium abundance of $\log N(\text{Cs})/N(\text{He}) = -5.45 \pm 0.35$, which can also be expressed in terms of the mass fraction $\log X_{\text{Cs}} = -3.95 \pm 0.35$.

Key words: atomic data – white dwarfs – stars: abundances – stars: individual: HD 149499B

1 INTRODUCTION

Because of their high gravity, white dwarfs are known to have atmospheres of either pure hydrogen or pure helium. Gravitational settling is so efficient in the atmospheres of these stars that element separation takes place rapidly in the absence of competing mixing mechanisms. The lightest element will float on the surface to form the atmosphere while the heavier will sink and disappear from sight. Although a small fraction of white dwarfs show traces of elements heavier than hydrogen and helium, the detection of trans-iron elements ($Z > 28$) in the spectra of the hot H-rich white dwarfs (DA) G191-B2B, Feige 24, and GD 246 by Vennes et al. (2005) and in the spectra of the hot He-rich white dwarfs (DO) HD 149499B and HZ 21 by Chayer et al. (2005) was unexpected as these elements have extremely low solar abundances (Asplund et al. 2009; Grevesse et al. 2015).

In a series of papers spanning almost a decade, T. Rauch, K. Werner, and collaborators reported the detection of several other trans-iron elements in the spectra of G191-B2B and the DO white dwarf RE 0503–289 (Rauch et al. 2012, 2014a,b, 2015a,b, 2016a,b, 2017a,b, 2020; Werner et al. 2012, 2018; Hoyer et al. 2017). They did not only identify these elements, but also calculated oscillator strengths for ionization stages IV–VII needed to determine the atmospheric abundances. This calculation was necessary to build

reliable stellar atmospheric models since, in most cases, only a small number of oscillator strengths were available in the literature (e.g., Morton 2000). By using these atomic data and a diffusion–radiative levitation code developed by Dreizler & Wolff (1999), Rauch et al. (2016a) demonstrated that radiative levitation can hold up trans-iron elements in the atmospheres of G191-B2B and RE 0503–289. They also elucidated, at least qualitatively, that the abundances in RE 0503–289 are higher than those in G191-B2B because of a higher effective temperature. Hoyer et al. (2018) extended the search for trans-iron elements in the atmospheres of two other DOs and a PG1159 star, and suggested that the abundance diversity was due to the effects of diffusion and radiative levitation. More recently, Löbling et al. (2020) discovered trans-iron elements in the DAO white dwarf BD–22°3467. It is interesting to note that all trans-iron elements observed in hot white dwarfs are overabundant.

Eighteen trans-iron elements have been so far identified in the atmospheres of hot white dwarfs: Cu ($Z = 29$), Zn (30), Ga (31), Ge (32), As (33), Se (34), Br (35), Kr (36), Sr (38), Zr (40), Mo (42), In (49), Sn (50), Sb (51), Te (52), I (53), Xe (54), and Ba (56). We can now add cesium ($Z = 55$) to this list as we have identified absorption lines of Cs IV, Cs V, and Cs VI in the *Far Ultraviolet Spectroscopic Explorer* (FUSE) spectrum of the DO HD 149499B. However, determining the Cs abundance poses a challenge similar to that encountered by T. Rauch, K. Werner, and collaborators in their analyses of trans-iron elements: the atomic data. Although Sansonetti (2009) compiled identified energy level structures and

* E-mail: chayer@stsci.edu

transition wavelengths for the whole Cs isonuclear sequence, and Husain et al. (2020) reported a critical evaluation of energy levels, wavelengths, and A -values for Cs vii, no transition probabilities for Cs iv–Cs vi have been measured or calculated to date. Consequently, our goal is to compute the respective oscillator strengths f_{ik} and transition probabilities A_{ki} for these species to determine the Cs abundance in the atmosphere of HD 149499B. Accurate radiative data are key to unravel the source of not only Cs but also of the other trans-iron elements observed in the atmospheres of hot white dwarfs.

In this paper we recount the calculation of the transition probabilities for Cs iv–Cs vi and the ensuing determination of the Cs abundance in the atmosphere of HD 149499B. The *FUSE* observations are described in Section 2. Section 3 summarises our approach to calculate the energy level structures and transition probabilities for these ions. A description of the cesium abundance analysis by means of stellar atmosphere models is presented in Section 4. We discuss our results and conclusions in Sections 5–6.

2 FAR-ULTRAVIOLET SPECTROSCOPY

2.1 *FUSE* Observations

FUSE is a space-based telescope launched in 1999 as part of NASA’s Origins program (Moos & et al. 2000) and deactivated in 2007. It is equipped with four independent spectrographs, two of which have LiF-coated optics sensitive to wavelengths between 990–1187 Å, and two have SiC-coated optics sensitive to wavelengths between 905–1104 Å. The average resolution of the spectrographs is $R \approx 20\,000$. Each spectrograph has a detector that records the signal on two independent microchannel-plate segments such that the spectral data are archived in eight files. The names of the segments and their wavelength coverage are: SiC1A (1004–1090 Å), SiC1B (905–993 Å), SiC2A (917–1005 Å), SiC2B (1016–1104 Å), LiF1A (988–1082 Å), LiF1B (1094–1187 Å), LiF2A (1087–1182 Å), and LiF2B (979–1075 Å).

As HD 149499B was chosen as a reliable target to check the stability of the *FUSE* photometric calibration, it was observed several times during the mission. Most of the observations were made under the photometric stability monitoring program M103 led by J. W. Kruk. All the spectra observed under program M103 and through the $30'' \times 30''$ aperture were retrieved from the Barbara A. Mikulski Archive for Space Telescope (MAST)¹. In total, thirteen observations using this aperture were made between 2000 and 2006. Since HD149499B is a bright star in the far-ultraviolet wavelength range, all data were recorded in spectral-image mode (histogram: HIST).

The spectral data for each segment were first co-aligned and then co-added by taking the average of all exposures weighted by their exposure times. The SiC1B, LiF1A, SiC2B, LiF2A, and LiF1B segments are merged to form the final spectrum. Exposure times vary slightly from segment to segment depending on the quality of the individual exposures. The average total exposure time is approximately 66 500 s. Given the number of co-added spectra and the star’s brightness, which is very close to the *FUSE* bright limit, the signal-to-noise ratio of the resulting spectrum is of exceptional quality for a *FUSE* spectrum. As the different segments have different sensitivities, the signal-to-noise ratio varies depending on the

wavelength. It is equal to 65, 98, and 161 at wavelengths 950, 1050, and 1150 Å.

2.2 Cesium detection

Considering the quality of the *FUSE* spectrum, HD 149499B shows interstellar and stellar absorption lines with equivalent widths as narrow as 2 mÅ. Wood et al. (2002) measured the deuterium abundance and that of other species toward HD 149499B by analysing the interstellar lines detected in the *FUSE* spectrum. They observed several absorption lines corresponding to ten species: H I, D I, C II, C III, N I, N II, O I, P II, Ar I, and Fe II. Chayer et al. (2005) for their part analysed the stellar lines, reporting the detection of C, Si, P, S, and also of several trans-iron elements such as Ge, As, Se, Sn, Te, and I. They reported the detection of the Br vi resonance line by using the wavelength published by Morton (2000), but it turned out, according to Werner et al. (2018), that this wavelength was incorrect and was in fact longer by 6.7 Å (Curtis et al. 1984). Werner et al. (2018) correctly identified the Br vi line in question, additionally identifying two other Br vi lines, and reported the first bromine detection in hot stars.

Although several interstellar and stellar species have been observed in the *FUSE* spectrum, there are still several absorption lines that have not yet been identified. The identification of cesium lines from the Cs iv, Cs v, and Cs vi species was possible by the publication of the observed spectral lines in the National Institute of Standards and Technology (NIST) Atomic Spectra Database² (Kramida et al. 2021). Thirteen cesium lines have been identified in the *FUSE* spectrum with equivalent widths in the range 2.3–26.9 mÅ. All these transitions arise from low-energy levels ranging from ten thousand to a few tens of thousands of cm^{−1}. These lines are listed in Table 1.

3 CESIUM ATOMIC DATA CALCULATIONS

The lack of oscillator strengths for Cs iv, Cs v, and Cs vi left us with no alternative but to calculate these data to estimate the cesium abundance in the atmosphere of HD149499B. The computation of the wave functions to determine A - and gf -values for atomic ions must take into account two important effects: electron correlation and the relativistic interactions. For multi-electron systems, the former is usually treated with configuration-interaction (CI) expansions (see, for instance, Weiss 1961), which for heavy systems such as cesium with open $n\ell$ shells ($n \geq 5$ and $\ell \leq 3$) show very slow convergence. The relativistic interaction, on the other hand, can be approximated with a Pauli Hamiltonian (one-body operators), a Breit–Pauli Hamiltonian (one- and two-body operators), or a full Dirac Hamiltonian. For the heavy systems, attaining high overall accuracy while accounting simultaneously for these two effects is a daunting task; thus, the ionic representations we have adopted for the present work may only be regarded as a reconnaissance visit. We use the multiconfiguration Breit–Pauli (MCBP) method for the bulk of the calculations and the multiconfiguration Dirac–Fock (MCDF) method to get a measure of the accuracy of the radiative data, particularly for the observed lines.

¹ <https://mast.stsci.edu/portal/Mashup/Clients/Mast/Portal.html>² <https://www.nist.gov/pml/atomic-spectra-database>

Table 1. Atomic and observed properties and abundances of photospheric Cs lines identified in the *FUSE* spectrum of HD 149499B.

Ion	Lab. (λ) (Å)	log g_f		E_i (cm $^{-1}$)	E.W. (mÅ)	log $N(\text{Cs})/N(\text{He})$		Comments
		MCBP	MCDF			MCBP	MCDF	
Cs IV	986.139	-1.022	-1.557	12902.0	2.3 ± 0.7	-6.09 ± 0.41	-5.54 ± 0.41	very faint line
	1068.905	-1.355	-2.084	20754.0	2.3 ± 0.3	-5.90 ± 0.50	-5.15 ± 0.50	very faint line
Cs V	925.857	-1.840	-1.770	31951.1	8.7 ± 0.8	-5.10 ± 0.37	-5.23 ± 0.37	next to ISM H I $\lambda 926$ line
	979.822	-0.942	-1.022	42273.7	15.1 ± 0.5	-5.99 ± 0.33	-5.92 ± 0.33	
Cs VI	1011.896	-1.253	-2.059	15077.4	23.9 ± 0.5	-5.92 ± 0.34	-5.10 ± 0.34	
	1064.881	-1.749	-2.119	31951.1	15.0 ± 0.6	-5.53 ± 0.34	-5.15 ± 0.34	line appears broader than model
Cs VII	1069.196	-1.429	-1.670	20373.5	26.9 ± 0.7	blend with Br V $\lambda 1069$ line
	971.049	-0.871	-1.039	35061.4	21.4 ± 0.9	blend with As IV $\lambda 971$ line
Cs VIII	982.436	-1.744	-1.933	52410.3	10.6 ± 0.7	-5.47 ± 0.34	-5.27 ± 0.34	next to unidentified weak line
	1020.117	-2.348	-2.592	35061.4	4.8 ± 0.3	uncertain identification
Cs IX	1034.069	-1.619	-1.712	35061.4	9.5 ± 0.6	-5.47 ± 0.34	-5.38 ± 0.34	
	1055.938	-1.621	-1.887	12176.0	23.8 ± 0.5	-5.31 ± 0.31	-5.04 ± 0.31	
Cs X	1120.444	-1.621	-1.830	17628.2	19.9 ± 0.4	-5.33 ± 0.32	-5.11 ± 0.32	next to I VI $\lambda 1120$ line and unidentified line
			Average [†] :		-5.61 ± 0.35	-5.29 ± 0.35		

[†] The average abundances can be expressed as mass fractions: $\log X_{\text{Cs}} = -4.11$ for MCBP and -3.79 for MCDF.**Table 2.** Electron configurations used in the present atomic models, where $n\ell = 5d, 6s, 6p, 6d, 7s$.

Cs IV	Cs V	Cs VI
5s ² 5p ⁴ , 5s5p ⁵ , 5p ⁶	5s ² 5p ³ , 5s5p ⁴ , 5p ⁵	5s ² 5p ² , 5s5p ³ , 5p ⁴
5s ² 5p ³ n ℓ	5s ² 5p ² n ℓ	5s ² 5pn ℓ
5s5p ⁴ n ℓ	5s5p ³ n ℓ	5s5p ² n ℓ
5p ⁵ n ℓ	5p ⁴ n ℓ	5p ³ n ℓ
5s ² 5p ² 5d ²	5s ² 5p5d ²	5s ² 5d ²
5s ² 5p ² 5d ⁶ s	5s ² 5p5d ⁶ s	5s ² 5d ⁶ s
5s ² 5p ² 6s ²	5s ² 5p6s ²	5s ² 6s ²
5s5p ³ 5d ²	5s5p ² 5d ²	5s5p5d ²
5s5p ³ 5d ⁶ s	5s5p ² 5d ⁶ s	5s5p5d ⁶ s
5s5p ³ 6s ²	5s5p ² 6s ²	5s5p6s ²
5p ⁴ 5d ²	5p ³ 5d ²	5p ² 5d ²
5p ⁴ 5d ⁶ s	5p ³ 5d ⁶ s	5p ² 5d ⁶ s
5p ⁴ 6s ²	5p ³ 6s ²	5p ² 6s ²

3.1 Multiconfiguration Breit–Pauli method

Wave functions for the Cs ionic models were obtained with the multiconfiguration Breit–Pauli (MCBP) method through a CI expansion of the form

$$\Psi(SLJ) = \sum_i c_i \psi(S_i L_i J) \quad (1)$$

using the AUTOSTRUCTURE atomic structure code (Eissner et al. 1974; Badnell 2011). The basic configuration functions $\psi(S_i L_i J)$ are built from $\phi(n\ell)$ one-electron orbitals obtained with the Thomas–Fermi–Dirac statistical model potential $V_{\text{mod}}(\lambda_{n\ell})$ of Eissner & Nussbaumer (1969), where the $\lambda_{n\ell}$ scaling parameters are variationally adjusted to minimize a weighted sum of the term energies of the ground and first-excited configurations. To obtain the radiative data, we performed modest calculations including only orbitals with principal quantum number $n \leq 7$ and orbital angular momentum $\ell \leq 2$. The configurations included in expansion (1) for each Cs ion are tabulated in Table 2.

The spectra of Cs VI, Cs V, and Cs IV listed in the NIST Atomic Spectra Database have been compiled by Sansonetti (2009) from the measurements by Tauheed et al. (1991), Tauheed & Joshi (1993), and Tauheed et al. (2005) who used a normal incidence spectro-

graph with a triggered spark. Level identification was based on CI structure calculations with the HFR Pauli code (Cowan 1981) and parametric least-squares fits. To reproduce these level structures and transition arrays, we have excluded configurations with 4f orbitals in the present atomic models.

The MCBP method relies on the relativistic Hamiltonian

$$H(R) = H(\text{NR}) + H(\text{BP}), \quad (2)$$

where $H(\text{NR})$ is the usual non-relativistic Hamiltonian and $H(\text{BP})$ contains the Breit–Pauli one- and two-body relativistic corrections (Eissner et al. 1974). Since Cs ions are large and complex, the CI expansions spanning the configurations listed in Table 2 are certainly non-convergent. To mitigate this shortcoming we introduce term energy corrections as described by Mendoza & Zeippen (1982). The relativistic wave function $\psi_i(R)$ may be expanded to first order in terms of the non-relativistic counterparts $\psi_i(\text{NR})$ as

$$\psi_i(R) = \psi_i(\text{NR}) + \sum_{j \neq i} \psi_j(\text{NR}) \cdot \frac{\langle \psi_j(\text{NR}) | H(\text{BP}) | \psi_i(\text{NR}) \rangle}{\Delta E_{ij}(\text{NR})}. \quad (3)$$

The term energy corrections (TEC)

$$\Delta E_{\text{nist}} = \Delta E_{ij}(\text{NR}) + \delta_i(\text{NR}) + \delta_j(\text{NR}) \quad (4)$$

are introduced in the Hamiltonian (2) and adjusted empirically such that the denominator of the summation in Eq. (3) is computed with the spectroscopic energy difference ΔE_{nist} listed in the NIST database.

3.2 Multiconfiguration Dirac–Fock method

To obtain a first estimate of g_f accuracy and a verification of level assignments, we performed a parallel calculation with the fully relativistic multi-configuration Dirac–Fock (MCDF) method (Grant et al. 1980; McKenzie et al. 1980) using the same configuration expansion of Table 2. The basic configuration functions $\psi(S_i L_i J)$ of Eq. (1) are now expressed as antisymmetrized products of the orthonormal monoelectronic spin-orbitals

$$\varphi_{nkm}(r, \theta, \phi) = \frac{1}{r} \left(\begin{array}{l} P_{nk}(r) \chi_{km}(\theta, \phi) \\ i Q_{nk}(r) \chi_{-km}(\theta, \phi) \end{array} \right), \quad (5)$$

where $P_{nk}(r)$ and $Q_{nk}(r)$ are the large and small radial orbitals, respectively, and the angular functions $\chi_{km}(\theta, \phi)$ are spinor spherical harmonics. These spin-orbitals are optimized self-consistently based on the Dirac–Coulomb Hamiltonian

$$H_{DC} = \sum_i c\vec{a}_i \cdot \vec{p}_i + \beta_i c^2 - \frac{Z}{r_i} + \sum_{i>j} \frac{1}{r_{ij}} \quad (6)$$

with the GRASP2K package (Parpia et al. 1996).

3.3 Energy levels

MCBP energy levels for Cs IV, Cs V, and Cs VI are respectively compared with the NIST spectroscopic measurements in Tables A1, A2, and A3 of Appendix A. Cs VI is the simpler spectrum with a $5s^25p^2$ ground configuration (see Table A3), whose energy differences with respect to NIST are within $\Delta E < 2000 \text{ cm}^{-1}$; i.e., less than 1%. The only inconsequential discrepancy is the configuration assignments of the strongly mixed 1D_2 levels, for which we find the leading percentages $(5s^25p5d, 5s5p^3) = (35, 27)$ for the lowest level while NIST lists $(5s5p^3, 5s^25p5d) = (32, 28)$. As mentioned in Section 3.1, the NIST level assignments have been obtained with the HFR code, which in our experience are sometimes faulty.

The level comparison for Cs IV ($5s^25p^4$ ground configuration) in Table A1 is not as satisfactory: $\Delta E < 3000 \text{ cm}^{-1}$ with respect to NIST exhibiting a few specific outliers:

- $5s^25p^35d {}^3D_2^0$. We find $\Delta E > 14000 \text{ cm}^{-1}$ for the two levels with this identification. These large discrepancies are difficult to explain and may be due to misquoted values by NIST.
- $5s^25p^35d {}^3D_3^0$. This level at $E_{\text{NIST}} = 190\,309.9 \text{ cm}^{-1}$ is very close ($\Delta E \approx 4600 \text{ cm}^{-1}$) to $5s^25p^36s {}^3D_3^0$, and thus, the level assignments may be ambiguous: our level order is in fact the inverse of NIST.
- $5s^25p^35d {}^3D_1^0$. This level at $E_{\text{NIST}} = 189\,391.7 \text{ cm}^{-1}$ is very close ($\Delta E \approx 3500 \text{ cm}^{-1}$) to $5s^25p^35d {}^3P_1^0$ whereby both levels showing strong admixture.

Regarding the energy level structure of Cs V ($5s^25p^3$ ground configuration), the situation is more complicated as the relativistic level admixture is stronger than in the two previously discussed ions, and as shown in the additional column of Table A2, our CI expansions suggest reassessments for the following NIST levels:

- $5s5p^4 {}^2S_{1/2}$, $5s5p^4 {}^2P_{1/2}$, and $5s^25p^25d {}^2P_{1/2}$
- $5s^25p^25d {}^4D_{5/2}$ and $5s^25p^25d {}^2F_{5/2}$
- $5s^25p^25d {}^4D_{7/2}$ and $5s^25p^25d {}^2F_{7/2}$
- $5s^25p^26s {}^2P_{3/2}$ and $5s^25p^25d {}^2P_{3/2}$
- $5s^25p^26s {}^2P_{1/2}$ and $5s^25p^25d {}^2S_{1/2}$.

Once these changes in level identifications are made, the energy differences between our computed energies and those of NIST are $\Delta E \lesssim 3000 \text{ cm}^{-1}$. Furthermore, Huo et al. (2017) have used the MCDF GRASP2K package to compute level energies for the ground configuration of Cs V. With the exception of the $5s^25p^3 {}^2P_{3/2}^0$ level, our MCBP values are marginally closer to NIST due to the fine-tuning procedure based on TEC (see Section 3.1).

3.4 Wavelengths

Radiative data for the allowed transition arrays of the three ions computed with the MCBP method are listed in Tables A4–A9. Regarding computed transition wavelengths, the best we can do is

exemplified with Cs VI (see Table A9), where the differences with the NIST wavelengths are on average $\overline{\Delta\lambda} = -0.1 \pm 2.4 \text{ \AA}$. The larger differences, $4.0 \leq \Delta\lambda \leq 8.5 \text{ \AA}$, occur in transitions with wavelengths $\lambda > 1000 \text{ \AA}$ involving the $5s^25p^2 {}^1D_2$ lower level.

For Cs IV, on the other hand, the wavelength comparison with NIST is poorer: $\overline{\Delta\lambda} = +0.1 \pm 15.1 \text{ \AA}$. However, if we exclude the transitions involving the two $5s^25p^35d {}^3D_2^0$ levels discussed in Section 3.3, then the average difference is reduced to a more acceptable $\overline{\Delta\lambda} = +0.5 \pm 7.0 \text{ \AA}$. Thus, in Table A5 we question the following NIST wavelengths: 558.161 \AA and 601.476 \AA of transition array 11 (TA-11); 586.848 \AA and 634.921 \AA of TA-17; 631.290 \AA of TA-35 and 589.776 \AA of TA-41.

The Cs V average wavelength difference with NIST is remarkable: $\overline{\Delta\lambda} = -2.3 \pm 7.1 \text{ \AA}$. Although the standard deviation is not larger than in Cs IV, the average difference indicates that the theoretical wavelength as a whole are shorter by $\sim 2 \text{ \AA}$. This is a symptom of the difficulties encountered when trying to fit a spectroscopic spectrum with TEC under pervasive level coupling.

3.5 Radiative rates and f -values

Tables A5, A7, and A9 tabulate MCBP A - and f -values for the allowed (E1) lines, and to the best of our knowledge, it is the first time that radiative rates are reported for these ionic species apart from the work by Biemont et al. (1995) on the forbidden (E2 and M1) lines within the ground configuration. Nonetheless, semi-empirical branching fractions have been previously estimated for the $5s^25p^2 - 5s^25p6s$ transition array by Curtis (2001). The F_2 and G_1 Slater parameters and ζ_p and ζ_{pp} spin-orbit energies where obtained by fitting the spectroscopic level energies to then derive singlet-triplet mixing angles and, hence, relative transition rates. In Table 3 we show a comparison of these branching fractions with those obtained from the present MCBP A -values. Regarding allowed lines with $\Delta S = 0$, the agreement for the ${}^3P^0 - {}^3P^0$ transitions is $\sim 20\%$ while significant discrepancies appear for ${}^1P_1^0 - {}^1D_2$ and ${}^1P_1^0 - {}^1S_0$, particularly a factor of 3 for the latter. For the intercombination transitions ($\Delta S \neq 0$), factor differences are found for ${}^3P_0^0 - {}^1S_0$ and ${}^1P_1^0 - {}^3P_1$.

Moreover, we compare the MCBP and MCDF g,f -values for the observed Cs lines in Table 1. The agreement is, as expected, relatively poor: within 0.3 dex apart from the three lines $\lambda\lambda 1986.139$, 1068.905, 1011.896 that display even larger discrepancies. The latter may be due to divergent CI expansions, strong admixture, and cancellation effects.

4 CESIUM ABUNDANCE ANALYSIS

We determine the cesium content of the star’s atmosphere by comparing the Cs lines observed in the HD 14949B FUSE spectrum with a grid of synthetic spectra. The grid is calculated for different Cs abundances and for a given effective temperature, gravity, and $N(\text{H})/N(\text{He})$ ratio. The synthetic spectra are themselves calculated from a grid of stellar atmosphere models that specify the physical properties of the upper layer of the star. We use the stellar atmosphere and spectrum synthesis codes Tlusty³ and Synspec⁴ to compute non-local thermodynamic equilibrium (non-LTE) stellar

³ <http://tlusty.oca.eu>

⁴ <http://tlusty.oca.eu/Synspec49/synspec.html>

Table 3. Comparison of branching fractions for the $5s^25p6s - 5s^25p^2$ transition array of Cs vi. BFP: present. BFC: [Curtis \(2001\)](#).

Upper level	Lower level	λ (Å)	BFP (%)	BFC (%)
5p6s $^3P_1^0$	5p 2 3P_0	410.31	26.4	31.0
	3P_1	431.89	15.1	15.6
	3P_2	442.30	41.4	51.2
	1D_2	479.25	2.0	1.8
	1S_0	522.72	16.9	0.3
5p6s $^3P_2^0$	5p 2 3P_1	401.97	24.5	27.7
	3P_2	410.98	46.2	51.1
	1D_2	442.69	29.3	21.2
5p6s $^1P_1^0$	5p 2 3P_0	378.46	0.1	0.6
	3P_1	396.75	1.4	4.4
	3P_2	405.52	9.0	11.9
	1D_2	436.37	49.4	68.6
	1S_0	472.11	40.1	14.6

atmosphere models and synthetic spectra of HD 149499B. A description of the two codes and their use is given in a series of three papers by [Hubeny & Lanz \(2017a,b,c\)](#).

4.1 Model atmospheres

As HD 149499B has a bright companion separated by only 2 arcsecs, no reliable optical spectroscopic study has thus far been performed ([Dreizler & Werner 1996](#)). We adopt the atmospheric parameters determined by [Napiwotzki et al. \(1995\)](#) in the analysis of the far-ultraviolet spectrum observed with the Berkeley spectrograph aboard the ORFEUS⁵ telescope. This spectrograph covers a wavelength range between 390 and 1170 Å with a resolution $R = \lambda/3000$. They fitted the stellar H I and He II lines observed beyond the Lyman edge at 912 Å with a grid of local thermodynamic equilibrium (LTE) stellar atmosphere models to determine the following stellar parameters: $T_{\text{eff}} = 49\,500 \pm 500$ K, $\log g = 7.97 \pm 0.08$, and $\log N(\text{H})/N(\text{He}) = -0.65 \pm 0.12$. [Jordan et al. \(1997\)](#) confirmed this temperature by analysing spectra collected by the *Extreme Ultraviolet Explorer*. By fitting the medium-wavelength (140–380 Å) and long-wavelength (280–760 Å) spectra, they estimated a temperature identical to that by [Napiwotzki et al. \(1995\)](#) and an interstellar hydrogen column density $N_{\text{H}} = 7 \times 10^{18} \text{ cm}^{-2}$ along the sight line of HD 149499B.

The model H and He atoms considered in our model atmosphere calculations are the same as those described by [Lanz & Hubeny \(2003, 2007\)](#), who calculated grids of non-LTE line-blanketed model atmospheres of B- and O-type stars. These model atoms are available from the Tlusty website⁶. Based on the atomic data calculated with the MCBP method described in Section 3.1 and those compiled by [Sansonetti \(2009\)](#), we built the cesium model atom following the description of [Hubeny & Lanz \(2017b,c\)](#). There is a model atom per cesium ion. We consider the Cs IV, Cs V, Cs VI, and Cs VII species. Each model atom consists of a set of energy levels and bound-free and bound-bound transitions. In order to keep a relatively small number of energy levels in the calculations, only the terms given in Tables A1, A2, and A3 are considered. This brings the number of energy levels to respectively 29,

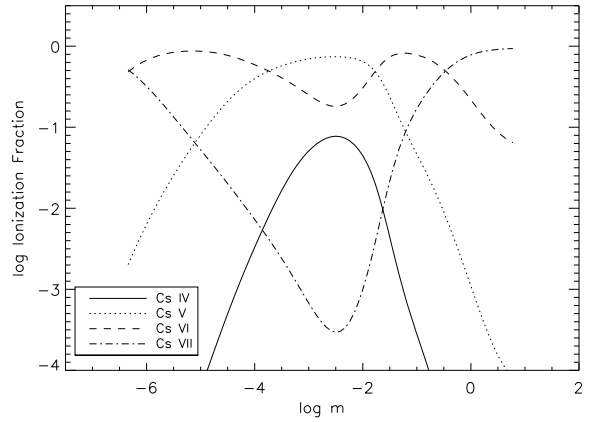


Figure 1. Ionization fractions of Cs IV–Cs VII as a function of the column mass $m (\text{g cm}^{-2})$ in a NLTE model of HD 149499B calculated with the atmospheric parameters provided by [Napiwotzki et al. \(1995\)](#): $T_{\text{eff}} = 49,500$ K, $\log g = 7.97$, and $\log N(\text{H})/N(\text{He}) = -0.65$.

22, and 17 for the Cs IV, Cs V, and Cs VI ions. Cs VII is considered as a single-energy level ion. Radiative bound–free transitions are described by hydrogenic cross sections, while collisional bound–free transitions are expressed in terms of photoionisation cross sections by the so-called [Seaton \(1962\)](#) formula. Allowed bound–bound transitions are described by depth-independent Doppler line profiles with a temperature given by $T = 0.75T_{\text{eff}}$. Total multiplet oscillator strengths f_{ik} are given in Tables A5, A7, and A9. For allowed line transitions, collisional excitation cross sections are computed using the [van Regemorter \(1962\)](#) formula, and for the forbidden line transitions, the cross sections are obtained by the [Eissner & Seaton \(1972\)](#) formula with $\gamma(T) = 0.5$.

We computed non-LTE stellar atmosphere models with a H, He, and Cs chemical composition. We considered the range of Cs abundances $\log N(\text{Cs})/N(\text{He}) = -9.6$ to -4.4 in steps of 0.4. We also computed models that take into account the uncertainties of the atmospheric parameters (ΔT_{eff} , $\Delta \log g$, $\Delta \log N(\text{H})/N(\text{He})$). The uncertainty on the effective temperature was increased to 2000 K to improve the assessment of the Cs abundance change with the effective temperature. Since the atmosphere of HD 149499B is rich in helium, the models were calculated by selecting the parameter IATREF = 2, which implies that helium was chosen as the reference atom. Fig. 1 compares the ionisation fractions of Cs in a model of HD 149499B showing that Cs V and Cs VI are the dominant ions in the line-forming region of the atmosphere, which is located between $\log m \approx -1.5$ and -4.0 . These ionisation fractions agree well with the detection of the Cs V and Cs VI lines in the *FUSE* spectrum of HD 149499B. The detection of weak Cs IV lines, which have $\log g f$ comparable to those of the Cs V and Cs VI, also illustrates that the ionisation fraction of Cs IV is about an order of magnitude lower than that of Cs V.

4.2 Spectral fitting

The Cs abundance is determined by comparing the cesium lines in the synthetic spectra to those observed in the *FUSE* spectrum. Synthetic spectra covering the *FUSE* wavelength range 905–1187 Å are calculated by using the spectral synthesis code *Synspec*. This code uses the models of stellar atmospheres calculated by Tlusty

⁵ Orbiting Retrievable Far and Extreme Ultraviolet Spectrometers

⁶ <http://tlusty.oca.eu/Tlusty2002/tlusty-frames-data.html>

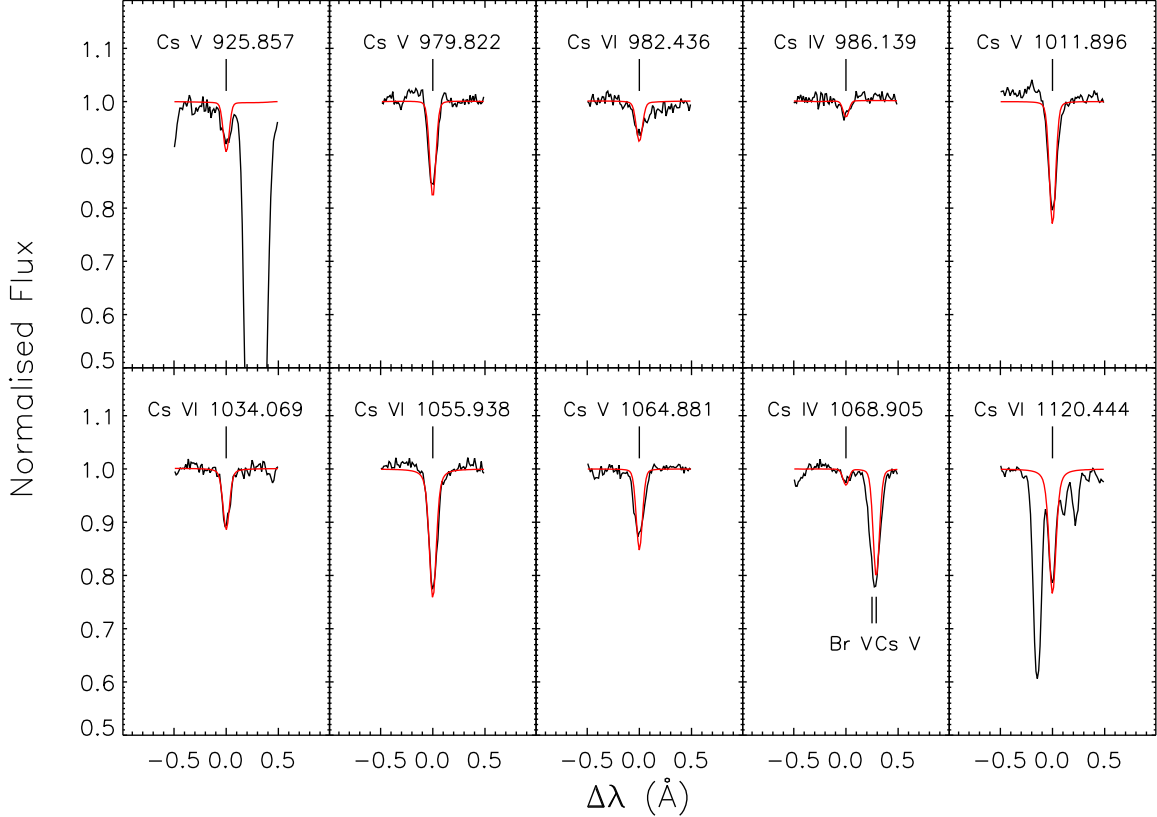


Figure 2. Best-fitting (red curves) to the Cs iv–Cs vi lines observed in the *FUSE* spectrum of HD 149499B (black curves). The fits are computed by considering the $\log g/f$ obtained by the MCBP method. Abundances are given in Table 1.

as input. The line list was retrieved from the Synspec website⁷ and supplemented with the Cs lines given in Tables A5, A7, and A9. The main Synspec output is the emergent flux listed in a table with the wavelength (\AA) and the flux expressed in terms of the flux moment, H_λ , in units of $\text{erg cm}^{-2} \text{s}^{-1} \text{\AA}^{-1}$. The synthetic spectra are convolved with a Gaussian of FWHM = 0.06 \AA such that their resolution matches that of *FUSE*; they are then normalised to the theoretical continuum provided by Synspec. Before making a comparison with the synthetic spectra, the observed lines are normalised and shifted to the laboratory rest frame. Using a fitting routine, the Cs abundance and its uncertainty are determined when the theoretical and observed lines match. The fitting routine calls a function that linearly interpolates among the synthetic spectra and fits them to each line individually by taking the abundance as a free parameter. Fig. 2 shows the best fits to the Cs iv–Cs vi lines.

4.3 Results: Cesium abundance

Table 1 lists the atomic and observed properties and abundances of the Cs iv–Cs vi lines detected in the *FUSE* spectrum. As described in Section 2 and illustrated in Fig. 2, the quality of the co-added *FUSE* spectrum allows the detection of very weak lines. For instance, the two detected Cs iv lines have equivalent widths of only 2.3 m \AA , and although these lines are very weak, they are clearly visible as shown in Fig. 2. A pair of lines are blended with known

lines: Cs v $\lambda 1069$ and Cs vi $\lambda 971$ with the Br v $\lambda 1069$ and As iv $\lambda 971$, respectively. The Cs vi $\lambda 1020$ line, on the other hand, appears to be blended with unidentified faint lines that slightly depress the continuum in the blue wing of the Lyman β and He ii $\lambda 1024$ lines. No Cs abundance was derived from these three lines.

Table 1 compares the oscillator strengths calculated with the MCBP and MCDF methods; it also gives the Cs abundances determined with these two datasets. The MCBP oscillator strengths are systematically larger than those calculated with MCDF. This results in abundances that are lower by a factor of two on average for the MCBP method. In both cases, the standard deviation of the abundance measurements for the ten lines is about 0.3 dex. The abundance uncertainties take into account those on the atmospheric parameters and the oscillator strengths and the quality of the fit. The uncertainties on the atmospheric parameters we have considered are $\Delta T_{\text{eff}} = 2\,000 \text{ K}$, $\Delta \log g = 0.08$, and $\Delta \log N(\text{H})/N(\text{He}) = 0.12$. The uncertainties on the oscillator strengths are estimated at 50%. On average, the contributions of these uncertainties to that on the abundance are: 0.16 dex for the effective temperature; 0.04 dex for the gravitational acceleration; 0.01 dex for the H abundance; 0.31 dex for the oscillator strength; and 0.04 dex for the statistical errors. The contributions of these uncertainties to the abundance uncertainty are combined in quadrature. The average abundances are $\log N(\text{Cs})/N(\text{He}) = -5.61 \pm 0.35$ and -5.29 ± 0.35 for the MCBP and MCDF methods, respectively. The corresponding mass fractions are $\log X_{\text{Cs}} = -4.11 \pm 0.35$ and -3.79 ± 0.35 . Taking the average of both methods, the Cs abundance and its mass fraction then become -5.45 ± 0.35 and -3.95 ± 0.35 .

⁷ <http://tlusty.oca.eu/Synspec49/synspec-frames-data.html>

5 DISCUSSION

5.1 Presence of cesium

Cesium detection in the atmosphere of HD 149449B is not surprising, because the list of trans-iron elements detected in the atmospheres of white dwarfs has grown considerably since that of germanium by Vennes et al. (2005). Cesium is now the nineteenth trans-iron element detected in the atmosphere of a white dwarf. Like other trans-iron elements observed in hot white dwarfs, cesium is overabundant by approximately 125,000 times solar. It is the most abundant trans-iron element in HD 149499B followed by bromine, iodine, selenium, arsenic, tin, tellurium, and germanium (Chayer et al. 2005; Werner et al. 2018). This cesium abundance is comparable, for instance, to other trans-iron elements observed in the hotter DO RE 0503–289 (Hoyer et al. 2018).

The presence of cesium and other trans-iron elements in the atmospheres of hot white dwarfs is remarkable. As white dwarfs are well known for their intense gravitational fields, a physical mechanism must counteract the effects of downward element diffusion to maintain these trans-iron elements in the atmosphere. In hot white dwarfs, radiative levitation is the natural mechanism to explain their presence (Vauclair et al. 1979; Chayer et al. 1995; Dreizler & Wolff 1999; Rauch et al. 2016a). The radiation field in these hot stars provides enough momentum through bound–bound absorption to allow the heavy elements to levitate in the atmosphere. As the momentum transferred to an element depends on its abundance, determination of the latter is possible when the radiative acceleration equals the gravitational acceleration. Based on the equilibrium radiative levitation theory, Rauch et al. (2016a) calculated equilibrium distributions of nine trans-iron elements at the surfaces of the DA G191–B2B and DO RE 0503–289. They demonstrated that radiative levitation can support trans-iron elements with equilibrium abundances showing overabundances in the line-forming regions. In future work, we intend to show that radiative levitation can maintain cesium in the atmosphere of HD 149499B.

5.2 Source of cesium

Could the presence of cesium in the atmosphere of HD 149499B indicate that lighter elements have undergone exposure to slow neutron capture (*s*-process) during previous phases of the star’s evolution? Models describing the evolution of asymptotic-giant-branch (AGB) stars show that *s*-process nucleosynthesis of trans-iron elements is possible for low- and intermediate-mass stars (Iben & Renzini 1983; Busso et al. 1999; Herwig 2005). The detection of these elements in the atmospheres of white dwarfs could then provide clues to understand better the role of *s*-process nucleosynthesis during the AGB phase. However, because diffusion processes such as gravitational settling and radiative levitation erase all traces of the abundance history, it is not possible to disentangle the trans-iron element abundances produced by *s*-process nucleosynthesis during the AGB phase from those present during star formation. Although radiative levitation complicates the interpretation of the source of trans-iron elements, it enables the buildup of large abundances, and therefore, the detection of those elements that otherwise would not be detected. As suggested by Werner et al. (2015), confirmation of *s*-process nucleosynthesis would entail the detection of a radioactive element such as technetium (Tc). The detection of this element in the atmosphere of red-giant stars by Merrill (1952) confirmed that *s*-process nucleosynthesis had taken place in evolved stars. In the case of hot white dwarfs, radiative

levitation would favor the detection of technetium even if it disintegrates over time. Technetium would diffuse from deeper regions in the atmosphere to the surface by radiative levitation, and would show an abundance when the radiative acceleration equals the gravitational acceleration. Ultimately, technetium would disappear from the atmosphere, but its disappearance would be delayed by radiative levitation.

5.3 Cesium atomic data

Computing radiative data for heavy ions such as Cs IV–Cs VI has been an interesting challenge. Ionic species with ground configurations $ns^2 np^m$ ($2 \leq n \leq 3$ and $2 \leq m \leq 4$) are familiar in nebular astrophysics, but the required A -values are mostly for line-ratio diagnostics involving forbidden lines. In the present study, $n = 5$, but conveniently, the level structures display similar symmetries simplifying the atomic representation strategies. However, for hot white-dwarf atmospheric models, the required radiative rates are for allowed transition arrays involving levels from the lowly excited configurations displaying 5d and 6s orbitals. Slow CI expansion convergence and strong relativistic couplings are then more difficult to account for to ensure acceptable accuracy.

We were surprised by the lack of previous A -value estimates despite the comprehensive Cs spectrum compilation by Sansonetti (2009), which includes well-identified spectroscopic level structures for Cs IV–Cs VI by Tauheed et al. (1991, 2005) and Tauheed & Joshi (1993). Such level identifications were based on HFR CI calculations, which for configurations of the type $nsnp^m$ ($3 \leq m \leq 5$) can be faulty as reported by Palmeri et al. (2012). The present level assignments resulting from adjusting the theoretical term energies to the spectroscopic values with TEC are expected to be more reliable. A problem that emerges in this procedure is that, due to strong relativistic couplings and level admixture, term splittings can be large; thus, *LS*-averaged wavelengths will not necessarily lead to adequate representations of the observed transition arrays.

Without comparisons with independent datasets, it is difficult to give an estimate of the accuracy level of the present radiative rates. In our attempt to reproduce the observed spectra, we kept our CI expansions as concise as possible, excluding for instance configurations with 4f orbitals. It is difficult to predict a priori whether this approximation leads to significant limitations. The comparison with the semi-empirical branching ratios for the $5s^2 5p^2 - 5s^2 5p6s$ transition array by Curtis (2001) showed nonetheless significant discrepancies that can be attributed to relativistic effects. We intend as a followup to the present report to recompute the present radiative datasets with a multiconfiguration Dirac–Fock method in an attempt to constrain accuracy ratings and to determine collision strengths and photoionisation cross sections with AUTOSTRUCTURE to improve the non-LTE atmospheric models. Therefore, from the atomic physics point of view, the present Cs abundance determinations is open to improvement.

6 CONCLUSION

The detection of cesium in the atmosphere of HD 149499B is the latest addition to a list of trans-iron elements observed in the atmospheres of hot white dwarfs. Absorption lines from Cs IV, Cs V, and Cs VI are present in the *FUSE* spectrum. First, we determined the oscillator strengths of the bound–bound transitions of these three ions using state-of-the-art atomic structure codes. We then determined the cesium abundance using stellar atmosphere models. With a mass

fraction of $\log X_{\text{Cs}} = -3.95 \pm 0.35$, cesium is the most abundant trans-iron element observed in HD 149499B. Radiative levitation is the most plausible natural phenomenon to explain its presence. Although radiative levitation favors its observation, it complicates the search of its origin.

ACKNOWLEDGEMENTS

This research has made use of the SIMBAD database, operated at CDS, Strasbourg, France. All of the astronomical observation data presented in this paper were obtained from the Mikulski Archive for Space Telescope (MAST). STScI is operated by the Association of Universities for Research in Astronomy, Inc., under NASA contract NAS5-26555. Support for MAST for non-HST data is provided by the NASA Office of Space Science via grant NNX13AC07G and by other grants and contracts. This research has made use of NASA's Astrophysics Data System.

DATA AVAILABILITY

The data underlying this article will be shared on reasonable request to the corresponding author.

REFERENCES

- Asplund M., Grevesse N., Sauval A. J., Scott P., 2009, *ARA&A*, **47**, 481
 Badnell N. R., 2011, *CoPhC*, **182**, 1528
 Biemont E., Hansen J. E., Quinet P., Zeippen C. J., 1995, *A&AS*, **111**, 333
 Busso M., Gallino R., Wasserburg G. J., 1999, *ARA&A*, **37**, 239
 Chayer P., Fontaine G., Wesemael F., 1995, *ApJS*, **99**, 189
 Chayer P., Vennes S., Dupuis J., Kruk J. W., 2005, *ApJ*, **630**, L169
 Cowan R. D., 1981, *The Theory of Atomic Structure and Spectra*. University of California, Berkeley
 Curtis L. J., 2001, *Phys. Scr.*, **63**, 104
 Curtis L. J., Martinson I., Leavitt J. A., Dietrich D. D., Bashkin S., Denne B., 1984, *Phys. Lett. A*, **105**, 212
 Dreizler S., Werner K., 1996, *A&A*, **314**, 217
 Dreizler S., Wolff B., 1999, *A&A*, **348**, 189
 Eissner W., Nussbaumer H., 1969, *J. Phys. B At. Mol. Phys.*, **2**, 1028
 Eissner W., Seaton M. J., 1972, *J. Phys. B At. Mol. Phys.*, **5**, 2187
 Eissner W., Jones M., Nussbaumer H., 1974, *CoPhC*, **8**, 270
 Grant I. P., McKenzie B. J., Norrington P. H., Mayers D. F., Pyper N. C., 1980, *CoPhC*, **21**, 207
 Grevesse N., Scott P., Asplund M., Sauval A. J., 2015, *A&A*, **573**, A27
 Herwig F., 2005, *ARA&A*, **43**, 435
 Hoyer D., Rauch T., Werner K., Kruk J. W., Quinet P., 2017, *A&A*, **598**, A135
 Hoyer D., Rauch T., Werner K., Kruk J. W., 2018, *A&A*, **612**, A62
 Hubeny I., Lanz T., 2017a, preprint, (arXiv:1706.01859),
 Hubeny I., Lanz T., 2017b, preprint, (arXiv:1706.01935),
 Hubeny I., Lanz T., 2017c, preprint, (arXiv:1706.01937),
 Huo X., Jiang G., Li X., 2017, *Can. J. Phys.*, **95**, 590
 Husain A., Haris K., Jabeen S., Tauheed A., 2020, *J. Quant. Spectrosc. Radiative Transfer*, **247**, 106956
 Iben I. J., Renzini A., 1983, *ARA&A*, **21**, 271
 Jordan S., Napiotzki R., Koester D., Rauch T., 1997, *A&A*, **318**, 461
 Kramida A., Yu. Ralchenko Reader J., and NIST ASD Team 2021, NIST Atomic Spectra Database (ver. 5.9), [Online]. Available: <https://physics.nist.gov/asd> [2022, September 24]. National Institute of Standards and Technology, Gaithersburg, MD.
 Lanz T., Hubeny I., 2003, *ApJS*, **146**, 417
 Lanz T., Hubeny I., 2007, *ApJS*, **169**, 83
 Löbling L., Maney M. A., Rauch T., Quinet P., Gamrath S., Kruk J. W., Werner K., 2020, *MNRAS*, **492**, 528
 McKenzie B. J., Grant I. P., Norrington P. H., 1980, *CoPhC*, **21**, 233
 Mendoza C., Zeippen C. J., 1982, *MNRAS*, **198**, 127
 Merrill P. W., 1952, *ApJ*, **116**, 21
 Moos H. W., et al. 2000, *ApJ*, **538**, L1
 Morton D. C., 2000, *ApJS*, **130**, 403
 Napiotzki R., Hurwitz M., Jordan S., Bowyer S., Koester D., Weidemann V., Lampton M., Edelstein J., 1995, *A&A*, **300**, L5
 Palmeri P., Quinet P., Mendoza C., Bautista M. A., García J., Witthoeft M. C., Kallman T. R., 2012, *A&A*, **543**, A44
 Parpia F. A., Fischer C. F., Grant I. P., 1996, *CoPhC*, **94**, 249
 Rauch T., Werner K., Biémont É., Quinet P., Kruk J. W., 2012, *A&A*, **546**, A55
 Rauch T., Werner K., Quinet P., Kruk J. W., 2014a, *A&A*, **564**, A41
 Rauch T., Werner K., Quinet P., Kruk J. W., 2014b, *A&A*, **566**, A10
 Rauch T., Werner K., Quinet P., Kruk J. W., 2015a, *A&A*, **577**, A6
 Rauch T., Hoyer D., Quinet P., Gallardo M., Raineri M., 2015b, *A&A*, **577**, A88
 Rauch T., Quinet P., Hoyer D., Werner K., Demleitner M., Kruk J. W., 2016a, *A&A*, **587**, A39
 Rauch T., Quinet P., Hoyer D., Werner K., Richter P., Kruk J. W., Demleitner M., 2016b, *A&A*, **590**, A128
 Rauch T., Gamrath S., Quinet P., Löbling L., Hoyer D., Werner K., Kruk J. W., Demleitner M., 2017a, *A&A*, **599**, A142
 Rauch T., Quinet P., Knörzer M., Hoyer D., Werner K., Kruk J. W., Demleitner M., 2017b, *A&A*, **606**, A105
 Rauch T., Gamrath S., Quinet P., Demleitner M., Knörzer M., Werner K., Kruk J. W., 2020, *A&A*, **637**, A4
 Sansonetti J. E., 2009, *J. Phys. Chem. Ref. Data*, **38**, 761
 Seaton M. J., 1962, in Bates D. R., ed., *Atomic and Molecular Processes*. p. 375
 Tauheed A., Joshi Y. N., 1993, *Phys. Scr.*, **47**, 550
 Tauheed A., Joshi Y. N., Kaufman V., 1991, *Phys. Scr.*, **44**, 579
 Tauheed A., Jabeen S., Joshi Y. N., 2005, *Phys. Scr.*, **71**, 193
 Vauclair G., Vauclair S., Greenstein J. L., 1979, *A&A*, **80**, 79
 Vennes S., Chayer P., Dupuis J., 2005, *ApJ*, **622**, L121
 Weiss A. W., 1961, *Phys. Rev.*, **122**, 1826
 Werner K., Rauch T., Ringat E., Kruk J. W., 2012, *ApJ*, **753**, L7
 Werner K., Rauch T., Kučas S., Kruk J. W., 2015, *A&A*, **574**, A29
 Werner K., Rauch T., Knörzer M., Kruk J. W., 2018, *A&A*, **614**, A96
 Wood B. E., Linsky J. L., Hébrard G., Vidal-Madjar A., Lemoine M., Moos H. W., Sembach K. R., Jenkins E. B., 2002, *ApJS*, **140**, 91
 van Regemorter H., 1962, *ApJ*, **136**, 906

APPENDIX A: CESIUM ATOMIC DATA

The present determination of the Cs abundance in the hot white dwarf HD 149499B required fairly extensive calculations of the level structures and radiative rates of Cs IV, Cs V, and Cs VI. In the following tables, we tabulate MCBP energy levels and A -, f -, and $\log(gf)$ -values for allowed transitions in these ionic species. MCBP and NIST energy levels for Cs IV, Cs V, and Cs VI are compared in Tables A1, A2, and A3. Atomic transition probabilities are given in Tables A5, A7, and A9. Finding lists ordered in increasing wavelengths are given in Tables A4, A6, and A8. These finding lists correspond to the atomic transitions that are reported in Tables A5, A7, and A9, respectively.

This paper has been typeset from a *TeX/LaTeX* file prepared by the author.

Table A1. Cs iv: Comparison of MCBP and NIST energy levels.

Configuration	Term	J	$E(\text{Present})$ (cm $^{-1}$)	$E(\text{NIST})$ (cm $^{-1}$)	Configuration	Term	J	$E(\text{Present})$ (cm $^{-1}$)	$E(\text{NIST})$ (cm $^{-1}$)
$5s^25p^4$	3P	2	0.0	0.0	$5s^25p^35d$	$^3D^o$	1	159501.2	162425.9
	3P	0	10001.8	9749.4		$^3D^o$	2	165031.1	179159.8
	3P	1	13353.5	12902.0		$^3D^o$	3	170539.7	173942.4
	term		5562.5	5383.9		term		166495.8	173378.2
$5s^25p^4$	1D	2	21069.1	20754.0	$5s^25p^35d$	$^3F^o$	3	175067.3	174789.4
	term		21069.1	20754.0		$^3F^o$	2	175677.9	174718.7
$5s^25p^4$	1S	0	43710.8	43279.4		$^3F^o$	4	179732.5	179872.0
	term		43710.8	43279.4		term		177212.1	176950.7
$5s5p^5$	$^3P^o$	2	115200.7	114307.7	$5s^25p^35d$	$^3P^o$	0	171181.9	169843.8
	$^3P^o$	1	121896.8	121242.5		$^3P^o$	1	171633.4	171449.5
	$^3P^o$	0	129149.6	128086.3		$^3P^o$	2	182208.5	182511.0
	term		118982.5	118150.2		term		177458.3	177416.4
$5s^25p^35d$	$^5D^o$	3	135947.2	135979.9	$5s^25p^35d$	$^3S^o$	1	179292.8	179477.8
	$^5D^o$	2	135951.3	136143.1		term		179292.8	179477.8
	$^5D^o$	1	136734.8	136868.6	$5s^25p^35d$	$^1F^o$	3	181748.3	180538.2
	$^5D^o$	0	136802.1	136625.7		term		181748.3	180538.2
	$^5D^o$	4	137422.4	136858.0	$5s^25p^36s$	$^3D^o$	2	181985.7	181944.8
	term		136607.7	136461.1		$^3D^o$	1	182132.6	182573.3
$5s^25p^35d$	$^1P^o$	1	139499.5	141402.9		$^3D^o$	3	187352.2	185718.8
	term		139499.5	141402.9		term		184519.5	183831.7
$5s^25p^35d$	$^3D^o$	2	142532.7	142167.0	$5s^25p^35d$	$^3D^o$	3	185126.8	190309.8
	$^3D^o$	3	147523.5	147695.5		$^3D^o$	2	191713.6	170401.9
	$^3D^o$	1	148711.1	148640.0		$^3D^o$	1	194102.1	189391.7
	term		146097.3	146041.6		term		189117.5	183490.2
$5s^25p^35d$	$^1S^o$	0	153085.8	152832.1	$5s^25p^35d$	$^3P^o$	2	184678.8	187266.6
	term		153085.8	152832.1		$^3P^o$	1	188531.7	185913.9
$5s^25p^35d$	$^3F^o$	2	150853.9	150982.7		$^3P^o$	0	196072.2	192952.0
	$^3F^o$	3	152645.0	152776.7		term		187229.0	187447.4
	$^3F^o$	4	158458.4	157759.0	$5s^25p^36s$	$^1D^o$	2	189086.6	189217.8
	term		154709.9	154484.8		term		189086.6	189217.8
$5s^25p^35d$	$^3G^o$	3	155138.5	155045.5	$5s5p^5$	$^1P^o$	1	197414.1	194685.9
	$^3G^o$	4	155156.1	154789.0		term		197414.1	194685.9
	$^3G^o$	5	160640.1	160328.0	$5s^25p^35d$	$^1D^o$	2	199531.3	197380.8
	term		157385.7	157112.1		term		199531.3	197380.8
$5s^25p^35d$	$^1G^o$	4	161345.2	160985.0	$5s^25p^35d$	$^1F^o$	3	200091.6	199392.1
	term		161345.2	160985.0		term		200091.6	199392.1
$5s^25p^36s$	$^5S^o$	2	164753.3	164609.5	$5s^25p^36s$	$^3P^o$	0	199707.1	198135.3
	term		164753.3	164609.5		$^3P^o$	1	200501.8	198514.1
$5s^25p^35d$	$^1D^o$	2	167662.6	166472.1		$^3P^o$	2	207033.6	207937.6
	term		167662.6	166472.1		term		204042.3	203707.3
$5s^25p^36s$	$^3S^o$	1	167404.0	167553.8	$5s^25p^36s$	$^1P^o$	1	208749.7	208500.0
	term		167404.0	167553.8		term		208749.7	208500.0
					$5s^25p^35d$	$^1P^o$	1	213754.0	213044.0
						term		213754.0	213044.0

Table A2. Cs v: Comparison of MCBP and NIST energy levels. In column E_{ra} (NIST) several NIST levels have been reassigned.

Conf	Term	J	$E(\text{Pres})$ (cm $^{-1}$)	$E_{\text{ra}}(\text{NIST})$ (cm $^{-1}$)	$E(\text{NIST})$ (cm $^{-1}$)	Conf	Term	J	$E(\text{Pres})$ (cm $^{-1}$)	$E_{\text{ra}}(\text{NIST})$ (cm $^{-1}$)	$E(\text{NIST})$ (cm $^{-1}$)
$5s^25p^3$	$^4S^o$	3/2	0.0	0.0	0.0	$5s^25p^25d$	2G	7/2	190802.0	189415.9	189415.9
$5s^25p^3$	$^2D^o$	3/2	15025.3	15077.4	15077.4		2G	9/2	193152.4	192876.3	192876.3
	$^2D^o$	5/2	20408.2	20373.5	20373.5		term		192107.8	191338.3	191338.3
	term		18255.0	18255.1	18255.1	$5s5p^4$	2P	3/2	191078.9	188245.8	188245.8
$5s^25p^3$	$^2P^o$	1/2	31717.5	31951.1	31951.1		2P	1/2	202678.7	201141.6	158248.8
	$^2P^o$	3/2	42390.5	42273.7	42273.7		term		194945.5	192544.4	178246.8
	term		38832.9	38832.8	38832.8	$5s^25p^25d$	2D	3/2	197001.3	195328.4	195328.4
$5s5p^4$	4P	5/2	113978.6	113901.7	113901.7		2D	5/2	204450.6	199403.5	199403.5
	4P	3/2	123527.9	123192.4	123192.4		term		201470.9	197773.4	197773.4
	4P	1/2	125631.5	125858.3	125858.3	$5s^25p^25d$	2D	3/2	208470.1	206375.9	206375.9
	term		119103.9	118991.4	118991.4		2D	5/2	209948.6	206712.0	206712.0
$5s5p^4$	2D	3/2	140111.1	139959.2	139959.2		term		209357.2	206577.6	206577.6
	2D	5/2	144290.8	144333.0	144333.0	$5s^25p^26s$	4P	1/2	201077.9	200123.6	200123.6
	term		142618.9	142583.5	142583.5		4P	3/2	209943.3	211476.1	211476.1
$5s5p^4$	2S	1/2	156392.5	158248.8	175576.8		4P	5/2	216635.2	217754.6	217754.6
	term		156392.5	158248.8	175576.8		term		211811.7	212723.3	212723.3
$5s^25p^25d$	2P	3/2	155043.5	154971.2	154971.2	$5s^25p^26s$	2P	3/2	215870.8	214163.1	221933.8
	2P	1/2	172834.9	175576.8	201141.6		2P	1/2	221884.9	220013.2	216635.5
	term		160974.0	161839.7	170361.3		term		217875.5	216113.2	220167.7
$5s^25p^25d$	4F	3/2	158095.5	157903.0	157903.0	$5s^25p^25d$	2D	5/2	210966.7	211084.4	211084.4
	4F	5/2	160233.8	160327.9	160327.9		2D	3/2	228842.4	223839.4	223839.4
	4F	7/2	166507.9	167231.1	167231.1		term		218117.0	216186.4	216186.4
	4F	9/2	172478.1	172717.1	172717.1	$5s^25p^25d$	2P	1/2	207510.2	205203.2	205203.2
	term		166093.9	166378.5	166378.5		2P	3/2	225816.6	221933.8	214163.1
$5s^25p^25d$	4D	1/2	165701.9	169557.9	169557.9		term		219714.5	216356.9	211176.5
	4D	5/2	168498.9	166800.2	175405.0	$5s^25p^25d$	2S	1/2	217324.7	216635.5	220013.2
	4D	3/2	169141.7	171936.6	171936.7		term		217324.7	216635.5	220013.2
	4D	7/2	171085.0	170736.7	184244.5	$5s^25p^25d$	2F	7/2	213969.6	217754.6	217754.6
	term		169382.2	169677.8	177662.4		2F	5/2	228341.8	224000.6	224000.6
$5s^25p^25d$	2F	5/2	175974.5	175405.0	166800.2		term		220129.1	220431.5	220431.5
	2F	7/2	184292.9	184244.5	170736.7	$5s^25p^26s$	2D	5/2	236507.1	235192.7	235192.7
	term		180727.9	180456.1	169049.6		2D	3/2	238208.2	237340.0	237340.0
$5s^25p^25d$	4P	5/2	188983.0	187619.8	187619.8		term		237187.6	236051.7	236051.7
	4P	3/2	192057.7	189992.1	189992.1						
	4P	1/2	192684.1	191236.7	191236.7						
	term		190624.7	189013.4	189013.4						

Table A3. Cs vi: Comparison of MCBP and NIST energy levels.

Configuration	Term	<i>J</i>	<i>E</i> (Present) (cm ⁻¹)	<i>E</i> (NIST) (cm ⁻¹)	Configuration	Term	<i>J</i>	<i>E</i> (Present) (cm ⁻¹)	<i>E</i> (NIST) (cm ⁻¹)
5s ² 5p ²	³ P	0	0.0	0.0	5s5p ³	¹ P ^o	1	195068.2	194461.0
	³ P	1	12543.7	12176.0		term		195068.2	194461.0
	³ P	2	18176.0	17628.2	5s ² 5p5d	³ P ^o	2	198040.8	197579.4
	term		14279.0	13852.1		³ P ^o	0	212559.6	212928.1
5s ² 5p ²	¹ D	2	36082.9	35061.4		³ P ^o	1	214569.6	214186.0
	term		36083.0	35061.4		term		205163.6	204820.3
5s ² 5p ²	¹ S	0	53158.3	52410.3	5s5p ³	¹ D ^o	2	209312.2	209795.3
	term		53158.3	52440.3		term		209312.2	209795.3
5s5p ³	⁵ S ^o	2	107475.2	106878.5	5s ² 5p5d	³ D ^o	1	201655.8	199798.6
	term		107475.2	106878.5		³ D ^o	3	213675.5	212146.6
5s5p ³	³ D ^o	1	132281.2	131766.8		³ D ^o	2	216514.9	216002.8
	³ D ^o	2	133684.7	133089.4		term		212218.0	210962.4
	³ D ^o	3	138755.4	138042.8	5s ² 5p5d	¹ F ^o	3	227087.8	226523.4
	term		135770.3	135136.5		term		227087.8	226523.4
5s5p ³	³ P ^o	0	152956.9	152634.7	5s ² 5p5d	¹ P ^o	1	232665.3	232014.9
	³ P ^o	1	154508.6	154198.2		term		232665.3	232014.9
	³ P ^o	2	155645.8	154775.8	5s ² 5p6s	³ P ^o	0	243444.9	242213.3
	term		154968.0	154345.4		³ P ^o	1	245712.0	243719.2
5s ² 5p5d	¹ D ^o	2	169521.8	168730.2		³ P ^o	2	260602.9	260952.0
	term		169521.8	168730.2		term		253732.8	253125.7
5s5p ³	³ S ^o	1	176445.8	175645.3	5s ² 5p6s	¹ P ^o	1	264952.7	264226.7
	term		176445.8	175645.3		term		264952.7	264226.7
5s ² 5p5d	³ F ^o	2	182782.8	181755.2					
	³ F ^o	3	188120.4	187270.0					
	³ F ^o	4	199124.3	198916.4					
	term		191565.5	190948.3					

Table A4. Cs iv: List of tabulated lines ordered in increasing wavelengths for allowed transitions that are given in Table A5.

Wavelength (Å)	No.						
469.387	25	566.165	45	630.026	38	734.521	2
479.616	24	566.605	17	630.726	13	735.403	2
480.913	23	567.164	19	631.129	41	736.714	4
491.897	25	567.651	18	631.290	35	744.648	31
499.645	25	572.117	12	633.696	10	757.445	30
501.524	22	572.349	12	634.921	17	759.570	3
503.143	24	573.511	18	637.179	13	767.879	30
503.742	23	574.903	11	644.186	62	773.605	4
506.635	21	574.938	44	644.972	7	778.205	3
511.253	24	577.995	18	646.614	10	780.213	56
512.727	23	578.624	16	649.201	36	781.946	29
513.648	20	583.262	13	649.499	36	786.663	2
520.048	49	586.848	17	651.169	9	787.764	29
525.459	17	589.051	64	652.791	35	804.671	54
528.006	17	589.177	14	654.550	6	806.669	2
528.492	19	589.375	16	654.979	11	808.253	2
529.760	23	589.591	13	659.163	8	811.418	2
532.634	48	589.776	41	660.474	61	823.635	29
533.998	18	591.566	16	662.327	6	824.793	1
534.235	47	592.987	41	663.590	37	828.851	28
537.883	18	593.599	43	668.789	11	839.303	55
538.449	16	596.823	10	672.767	4	861.218	27
538.758	23	600.328	14	677.069	4	866.633	27
539.860	23	600.555	42	681.199	34	867.860	27
540.726	20	600.701	9	684.405	59	868.174	1
542.068	21	601.476	11	686.257	33	874.832	1
547.725	16	605.251	63	695.142	32	896.916	1
547.912	13	605.474	42	701.093	60	923.016	1
549.617	16	606.190	40	703.398	4	949.122	53
550.104	20	607.498	8	705.856	35	986.139	1
553.899	15	615.665	11	707.199	3	995.138	26
555.401	18	617.973	40	714.642	5	1019.124	52
556.662	17	617.983	12	717.907	58	1068.500	51
557.173	14	618.211	37	719.991	4	1068.905	26
558.161	11	618.429	13	724.214	6	1282.658	50
559.791	46	620.383	40	730.628	2		
562.556	47	625.844	39	734.224	57		

Table A5. Cs iv: Allowed transitions (values of A_{ki} and f_{ik} are given with the notation $a \pm b \equiv a \times 10^{\pm b}$).

No.	Transition Array	Mult.	λ_{vac} (Å)	E_i (cm $^{-1}$)	E_k (cm $^{-1}$)	$g_i - g_k$	A_{ki} (10 8 s $^{-1}$)	f_{ik}	$\log g f$
1.	$5s^2 5p^4 - 5s 5p^5$	${}^3P - {}^3P^\circ$	886.789	5383.9	118150.2	9–9	5.230+00	6.097–02	−0.261
			874.832	0.0	114307.7	5–5	3.729+00	4.212–02	−0.677
			824.793	0.0	121242.5	5–3	3.416+00	2.068–02	−0.985
			896.916	9749.4	121242.5	1–3	1.366+00	4.908–02	−1.309
			986.139	12902.0	114307.7	3–5	1.314+00	3.166–02	−1.022
			923.016	12902.0	121242.5	3–3	1.088+00	1.384–02	−1.382
			868.174	12902.0	128086.3	3–1	4.230+00	1.576–02	−1.325
2.	$5s^2 5p^4 - 5s^2 5p^3 5d$	${}^3P - {}^5D^\circ$	762.909	5383.9	136461.1	9–25	6.633–01	1.613–02	−0.838
			735.403	0.0	135979.9	5–7	5.146–01	5.844–03	−1.534
			734.521	0.0	136143.1	5–5	1.001+00	8.122–03	−1.391
			730.628	0.0	136868.6	5–3	1.508+00	7.254–03	−1.440
			786.663	9749.4	136868.6	1–3	2.861–01	8.012–03	−2.096
			811.418	12902.0	136143.1	3–5	1.058–02	1.759–04	−3.278
			806.669	12902.0	136868.6	3–3	4.320–01	4.253–03	−1.894
			808.253	12902.0	136625.7	3–1	2.001+00	6.560–03	−1.706
3.	$5s^2 5p^4 - 5s^2 5p^3 5d$	${}^3P - {}^1P^\circ$	735.191	5383.9	141402.9	9–3	8.838–01	2.465–03	−1.654
			707.199	0.0	141402.9	5–3	3.430–01	1.586–03	−2.101
			759.570	9749.4	141402.9	1–3	3.536–01	9.483–03	−2.023
4.	$5s^2 5p^4 - 5s^2 5p^3 5d$	${}^3P - {}^3D^\circ$	710.946	5383.9	146041.6	9–15	1.316+00	1.659–02	−0.826
			703.398	0.0	142167.0	5–5	1.905+00	1.406–02	−1.153
			677.069	0.0	147695.5	5–7	9.599–01	9.258–03	−1.335
			672.767	0.0	148640.0	5–3	5.221–01	2.124–03	−1.974
			719.991	9749.4	148640.0	1–3	6.857–01	1.603–02	−1.795
			773.605	12902.0	142167.0	3–5	4.003–03	5.993–05	−3.745
			736.714	12902.0	148640.0	3–3	3.622–01	2.964–03	−2.051
5.	$5s^2 5p^4 - 5s^2 5p^3 5d$	${}^3P - {}^1S^\circ$	678.204	5383.9	152832.1	9–1	5.932–02	4.558–05	−3.387
			714.642	12092.0	152832.1	3–1	5.070–02	1.298–04	−3.410
6.	$5s^2 5p^4 - 5s^2 5p^3 5d$	${}^3P - {}^3F^\circ$	670.687	5383.9	154484.8	9–21	5.448–01	8.589–03	−1.112
			662.327	0.0	150982.7	5–5	1.130+00	7.446–03	−1.429
			654.550	0.0	152776.7	5–7	9.148–01	8.240–03	−1.385
7.	$5s^2 5p^4 - 5s^2 5p^3 5d$	${}^3P - {}^3G^\circ$	724.214	12902.0	150982.7	3–5	7.541–03	9.967–05	−3.524
			644.972	0.0	155045.5	5–7	3.625+00	3.160–02	−0.801
			659.073	5383.9	157112.1	9–27	8.808–01	1.718–02	−0.811
8.	$5s^2 5p^4 - 5s^2 5p^3 6s$	${}^3P - {}^5S^\circ$	628.040	5383.9	164609.5	9–5	5.439+00	1.786–02	−0.794
			607.498	0.0	164609.5	5–5	4.973+00	2.746–02	−0.862
			659.163	12902.0	164609.5	3–5	8.119–01	8.850–03	−1.576
9.	$5s^2 5p^4 - 5s^2 5p^3 5d$	${}^3P - {}^1D^\circ$	620.778	5383.9	166472.1	9–5	2.671+00	8.490–03	−1.117
			600.701	0.0	166472.1	5–5	2.065–01	1.101–03	−2.259
			651.169	12902.0	166472.1	3–5	2.152+00	2.259–02	−1.169

Table A5 – continued

No.	Transition Array	Mult.	λ_{vac} (Å)	E_i (cm $^{-1}$)	E_k (cm $^{-1}$)	g_{i-gk}	A_{ki} (10 8 s $^{-1}$)	f_{ik}	$\log g f$
10.	$5s^2 5p^4 - 5s^2 5p^3 6s$	${}^3P - {}^3S^\circ$	616.637	5383.9	167553.8	9–3	4.224+00	8.050–03	–1.140
				596.823	0.0	167553.8	5–3	3.083+00	9.896–03
				633.696	9749.4	167553.8	1–3	1.215+00	2.205–02
				646.614	12902.0	167553.8	3–3	9.564–02	6.040–04
11.	$5s^2 5p^4 - 5s^2 5p^3 5d$	${}^3P - {}^3D^\circ$	595.258	5383.9	173378.2	9–15	6.201+00	5.932–02	–0.273
				615.665	0.0	162425.9	5–3	9.192–01	3.250–03
				574.903	0.0	173942.4	5–7	5.448+00	3.932–02
				558.161	0.0	179159.8	5–5	2.171+00	1.195–02
				601.476	12092.0	179159.8	3–5	2.929+00	3.181–02
				654.979	9749.4	162425.9	1–3	7.372+00	1.483–01
12.	$5s^2 5p^4 - 5s^2 5p^3 5d$	${}^3P - {}^3F^\circ$	582.863	5383.9	176950.8	9–21	3.956+00	4.679–02	–0.376
				572.117	0.0	174789.4	5–7	6.094+00	4.174–02
				572.349	0.0	174718.7	5–5	7.561–01	3.672–03
				617.983	12902.0	174718.7	3–5	6.572+00	6.233–02
13.	$5s^2 5p^4 - 5s^2 5p^3 5d$	${}^3P - {}^3P^\circ$	581.285	5383.9	177416.4	9–9	1.022+02	5.187–01	0.669
				583.262	0.0	171449.5	5–3	6.838+01	2.088–01
				547.912	0.0	182511.0	5–5	1.293+02	5.838–01
				618.429	9749.4	171449.5	1–3	1.370+01	2.358–01
				637.179	12902.0	169843.8	3–1	1.092+01	2.190–02
				630.726	12902.0	171449.5	3–3	2.309+01	1.381–01
				589.591	12902.0	182511.0	3–5	3.611+00	3.164–02
14.	$5s^2 5p^4 - 5s^2 5p^3 5d$	${}^3P - {}^3S^\circ$	574.403	5383.9	179477.8	9–3	1.440+02	2.380–01	0.331
				557.173	0.0	179477.8	5–3	1.434+02	4.014–01
				589.177	9749.4	179477.8	1–3	1.094+01	1.716–01
				600.328	12902.0	179477.8	3–3	1.131+00	6.157–03
15.	$5s^2 5p^4 - 5s^2 5p^3 5d$	${}^3P - {}^1F^\circ$	570.925	5383.9	180538.2	9–7	1.264+01	4.741–02	–0.370
				553.899	0.0	180538.2	5–7	1.384+01	8.796–02
16.	$5s^2 5p^4 - 5s^2 5p^3 6s$	${}^3P - {}^3D^\circ$	560.388	5383.9	183831.7	9–15	2.677+01	2.114–01	0.279
				549.617	0.0	181944.8	5–5	1.009+01	4.566–02
				547.725	0.0	182573.3	5–3	4.825+01	1.308–01
				538.449	0.0	185718.8	5–7	6.357–02	3.800–04
				578.624	9749.4	182573.3	1–3	1.765+00	2.679–02
				589.375	12902.0	182573.3	3–3	4.446+01	2.340–01
				591.566	12902.0	181944.8	3–5	9.749+00	8.567–02
17.	$5s^2 5p^4 - 5s^2 5p^3 5d$	${}^3P - {}^3D^\circ$	561.463	5383.9	183490.2	9–15	2.817+02	2.101+00	1.277
				525.459	0.0	190309.8	5–7	3.599+02	2.204+00
				528.006	0.0	189391.7	5–3	7.002–01	1.672–03
				586.848	0.0	170401.9	5–5	6.926+00	2.826–02
				556.662	9749.4	189391.7	1–3	2.311+02	3.067+00
				634.921	12902.0	170401.9	3–5	1.860+02	1.461+00
				566.605	12902.0	189391.7	3–3	3.178+01	1.459–01
									–0.359

Table A5 – continued

No.	Transition Array	Mult.	λ_{vac} (Å)	E_i (cm $^{-1}$)	E_k (cm $^{-1}$)	$g_i - g_k$	A_{ki} (10 8 s $^{-1}$)	f_{ik}	$\log g f$
18.	$5s^2 5p^4 - 5s^2 5p^3 5d$	${}^3P - {}^3P^\circ$	549.259	5383.9	187447.4	9–9	2.579+02	1.166+00	1.021
			533.998	0.0	187266.6	5–5	2.286+02	1.005+00	0.701
			537.883	0.0	185913.9	5–3	1.019+02	2.580–01	0.111
			567.651	9749.4	185913.9	1–3	9.469+01	1.336+00	0.126
			573.511	12902.0	187266.6	3–5	4.621+00	3.933–02	–0.928
			577.995	12902.0	185913.9	3–3	8.719+01	4.260–01	0.107
			555.401	12902.0	192952.0	3–1	3.282+02	4.913–01	0.168
19.	$5s^2 5p^4 - 5s^2 5p^3 6s$	${}^3P - {}^1D^\circ$	543.970	5383.9	189217.8	9–5	2.099+01	5.209–02	–0.329
			528.492	0.0	189217.8	5–5	4.455–01	1.868–03	–2.030
			567.164	12902.0	189217.8	3–5	1.816+01	1.470–01	–0.356
20.	$5s^2 5p^4 - 5s 5p^5$	${}^3P - {}^1P^\circ$	528.256	5383.9	194685.9	9–3	1.552+02	2.110–01	0.279
			513.648	0.0	194685.9	5–3	3.446+00	7.954–03	–1.400
			540.726	9749.4	194685.9	1–3	1.103+00	1.413–02	–1.850
			550.104	12902.0	194685.9	3–3	1.336+02	5.910–01	0.249
21.	$5s^2 5p^4 - 5s^2 5p^3 5d$	${}^3P - {}^1D^\circ$	520.842	5383.9	197380.8	9–5	1.585+02	3.514–01	0.500
			506.635	0.0	197380.8	5–5	5.238+00	1.972–02	–1.006
			542.068	12902.0	197380.8	3–5	1.363+02	9.823–01	0.469
22.	$5s^2 5p^4 - 5s^2 5p^3 5d$	${}^3P - {}^1F^\circ$	515.442	5383.9	199392.1	9–7	4.450+00	1.369–02	–0.909
			501.524	0.0	199392.1	5–7	4.831+00	2.532–02	–0.898
23.	$5s^2 5p^4 - 5s^2 5p^3 6s$	${}^3P - {}^3P^\circ$	504.227	5383.9	203707.3	9–9	2.613+01	9.830–02	–0.053
			503.742	0.0	198514.1	5–3	1.579+00	3.534–03	–1.753
			480.913	0.0	207937.6	5–5	5.283–02	1.848–04	–3.034
			529.760	9749.4	198514.1	1–3	9.378+00	1.162–01	–0.935
			539.860	12902.0	198135.3	3–1	5.671+01	8.160–02	–0.611
			538.758	12902.0	198514.1	3–3	2.990+01	1.280–01	–0.416
			512.727	12902.0	207937.6	3–5	3.528+00	2.350–02	–1.152
24.	$5s^2 5p^4 - 5s^2 5p^3 6s$	${}^3P - {}^1P^\circ$	492.329	5383.9	208500.0	9–3	6.238+00	7.569–03	–1.167
			479.616	0.0	208500.0	5–3	2.599–01	5.364–04	–2.572
			503.143	9749.4	208500.0	1–3	6.403–01	7.291–03	–2.137
			511.253	12902.0	208500.0	3–3	4.746+00	1.864–02	–1.253
25.	$5s^2 5p^4 - 5s^2 5p^3 5d$	${}^3P - {}^1P^\circ$	481.556	5383.9	213044.0	9–3	6.584+00	7.608–03	–1.164
			469.387	0.0	213044.0	5–3	1.552–01	3.056–04	–2.816
			491.897	9749.4	213044.0	1–3	4.762–01	5.159–03	–2.287
			499.645	12902.0	213044.0	3–3	5.311+00	1.983–02	–1.226
26.	$5s^2 5p^4 - 5s 5p^5$	${}^1D - {}^3P^\circ$	1026.733	20754.0	118150.2	5–9	4.841–01	1.362–02	–1.167
			1068.905	20754.0	114307.7	5–5	4.910–01	8.308–03	–1.382
			995.138	20754.0	121242.5	5–3	5.808–01	5.138–03	–1.590
27.	$5s^2 5p^4 - 5s^2 5p^3 5d$	${}^1D - {}^5D^\circ$	864.251	20754.0	136461.1	5–25	3.754–03	2.119–04	–2.975
			867.860	20754.0	135979.9	5–7	2.336–03	3.716–05	–3.731
			866.633	20754.0	136143.1	5–5	1.184–02	1.345–04	–3.172
			861.218	20754.0	136868.6	5–3	5.933–03	3.989–05	–3.700

Table A5 – continued

No.	Transition Array	Mult.	λ_{vac} (Å)	E_i (cm $^{-1}$)	E_k (cm $^{-1}$)	g_{i-gk}	A_{ki} (10 8 s $^{-1}$)	f_{ik}	$\log g f$
28.	$5s^25p^4 - 5s^25p^35d$	${}^1D - {}^1P^\circ$	828.851	20754.0	141402.9	5–3	5.709+00	3.662–02	–0.737
29.	$5s^25p^4 - 5s^25p^35d$	${}^1D - {}^3D^\circ$	798.164	20754.0	146041.6	5–15	2.768–02	7.930–04	–2.402
			823.635	20754.0	142167.0	5–5	6.335–02	6.438–04	–2.492
			787.764	20754.0	147695.5	5–7	1.128–04	1.480–06	–5.131
			781.946	20754.0	148640.0	5–3	2.353–02	1.299–04	–3.187
30.	$5s^25p^4 - 5s^25p^35d$	${}^1D - {}^3F^\circ$	747.771	20754.0	154484.8	5–21	3.763–02	1.334–03	–2.176
			767.879	20754.0	150982.7	5–5	3.776–03	3.360–05	–3.775
			757.445	20754.0	152776.7	5–7	1.058–01	1.283–03	–2.193
31.	$5s^25p^4 - 5s^25p^35d$	${}^1D - {}^3G^\circ$	733.363	20754.0	157112.1	5–27	1.386–01	6.054–03	–1.519
			744.648	20754.0	155045.5	5–7	5.106–01	5.962–03	–1.526
32.	$5s^25p^4 - 5s^25p^36s$	${}^1D - {}^5S^\circ$	695.142	20754.0	164609.5	5–5	3.722–02	2.704–04	–2.869
33.	$5s^25p^4 - 5s^25p^35d$	${}^1D - {}^1D^\circ$	686.257	20754.0	166472.1	5–5	2.845–03	1.985–05	–4.003
34.	$5s^25p^4 - 5s^25p^36s$	${}^1D - {}^3S^\circ$	681.199	20754.0	167553.8	5–3	3.984–02	1.673–04	–3.077
35.	$5s^25p^4 - 5s^25p^35d$	${}^1D - {}^3D^\circ$	655.204	20754.0	173378.2	5–15	1.973+00	4.173–02	–0.681
			705.856	20754.0	162425.9	5–3	1.364+00	6.400–03	–1.495
			652.791	20754.0	173942.4	5–7	2.321+00	2.180–02	–0.963
			631.290	20754.0	179159.8	5–5	1.882+00	1.362–02	–1.167
36.	$5s^25p^4 - 5s^25p^35d$	${}^1D - {}^3F^\circ$	640.218	20754.0	176950.7	5–21	4.149+00	1.069–01	–0.272
			649.201	20754.0	174789.4	5–7	8.365+00	7.404–02	–0.432
			649.499	20754.0	174718.7	5–5	4.993+00	3.132–02	–0.805
37.	$5s^25p^4 - 5s^25p^35d$	${}^1D - {}^3P^\circ$	638.315	20754.0	177416.4	5–9	4.055–01	4.474–03	–1.650
			663.590	20754.0	171449.5	5–3	7.767–01	3.082–03	–1.812
			618.211	20754.0	182511.0	5–5	2.270–01	1.311–03	–2.183
38.	$5s^25p^4 - 5s^25p^35d$	${}^1D - {}^3S^\circ$	630.026	20754.0	179477.8	5–3	9.698+00	3.484–02	–0.759
39.	$5s^25p^4 - 5s^25p^35d$	${}^1D - {}^1F^\circ$	625.844	20754.0	180538.2	5–7	2.801+00	2.278–02	–0.943
40.	$5s^25p^4 - 5s^25p^36s$	${}^1D - {}^3D^\circ$	613.205	20754.0	183831.7	5–15	5.845+00	9.866–02	–0.307
			620.383	20754.0	181944.8	5–5	4.032–02	2.334–04	–2.933
			617.973	20754.0	182573.3	5–3	1.550+01	5.376–02	–0.571
			606.190	20754.0	185718.8	5–7	5.897+00	4.476–02	–0.650
41.	$5s^25p^4 - 5s^25p^35d$	${}^1D - {}^3D^\circ$	609.129	20754.0	184922.8	5–15	5.088+01	8.297–01	0.618
			631.129	20754.0	179159.8	5–7	3.341+00	2.606–02	–0.885
			589.776	20754.0	190309.8	5–5	1.267+02	6.520–01	0.513
			592.987	20754.0	189391.7	5–3	5.861+01	1.761–01	–0.055

Table A5 – continued

No.	Transition Array	Mult.	λ_{vac} (Å)	E_i (cm $^{-1}$)	E_k (cm $^{-1}$)	$g_i - g_k$	A_{ki} (10 8 s $^{-1}$)	f_{ik}	$\log g f$
42.	$5s^2 5p^4 - 5s^2 5p^3 5d$	${}^1D - {}^3P^\circ$	599.904	20754.0	187447.4	5–9	2.509+01	2.372–01	0.074
			600.555	20754.0	187266.6	5–5	7.208–01	4.038–03	–1.695
			605.474	20754.0	185913.9	5–3	7.204+01	2.310–01	0.063
43.	$5s^2 5p^4 - 5s^2 5p^3 6s$	${}^1D - {}^1D^\circ$	593.599	20754.0	189217.8	5–5	3.339+01	1.773–01	–0.052
44.	$5s^2 5p^4 - 5s 5p^5$	${}^1D - {}^1P^\circ$	574.938	20754.0	194685.9	5–3	1.517+02	4.388–01	0.341
45.	$5s^2 5p^4 - 5s^2 5p^3 5d$	${}^1D - {}^1D^\circ$	566.165	20754.0	197380.8	5–5	1.510+02	7.106–01	0.551
46.	$5s^2 5p^4 - 5s^2 5p^3 5d$	${}^1D - {}^1F^\circ$	559.791	20754.0	199392.1	5–7	3.384+02	2.216+00	1.045
47.	$5s^2 5p^4 - 5s^2 5p^3 6s$	${}^1D - {}^3P^\circ$	546.588	20754.0	203707.3	5–9	1.778+01	1.424–01	–0.148
			562.556	20754.0	198514.1	5–3	3.099+01	8.658–02	–0.364
			534.235	20754.0	207937.6	5–5	1.257+01	5.450–02	–0.565
48.	$5s^2 5p^4 - 5s^2 5p^3 6s$	${}^1D - {}^1P^\circ$	532.634	20754.0	208500.0	5–3	2.398+00	6.124–03	–1.514
49.	$5s^2 5p^4 - 5s^2 5p^3 5d$	${}^1D - {}^1P^\circ$	520.048	20754.0	213044.0	5–3	1.647+00	3.990–03	–1.700
50.	$5s^2 5p^4 - 5s 5p^5$	${}^1S - {}^3P^\circ$	1335.632	43279.4	118150.2	1–9	2.125–02	5.086–03	–2.294
			1282.658	43279.4	121242.5	1–3	7.198–02	5.296–03	–2.276
51.	$5s^2 5p^4 - 5s^2 5p^3 5d$	${}^1S - {}^5D^\circ$	1073.172	43279.4	136461.1	1–25	1.858–03	8.119–04	–3.091
			1068.500	43279.4	136868.6	1–3	1.569–02	8.154–04	–3.089
52.	$5s^2 5p^4 - 5s^2 5p^3 5d$	${}^1S - {}^1P^\circ$	1019.124	43279.4	141402.9	1–3	2.741–01	1.344–02	–1.872
53.	$5s^2 5p^4 - 5s^2 5p^3 5d$	${}^1S - {}^3D^\circ$	973.121	43279.4	146041.6	1–15	1.704–03	3.654–04	–3.437
			949.122	43279.4	148640.0	1–3	9.183–03	3.746–04	–3.426
54.	$5s^2 5p^4 - 5s^2 5p^3 6s$	${}^1S - {}^3S^\circ$	804.671	43279.4	167553.8	1–3	5.905–04	1.736–05	–4.760
55.	$5s^2 5p^4 - 5s^2 5p^3 5d$	${}^1S - {}^3D^\circ$	768.646	43279.4	173378.2	1–15	2.755–02	3.876–03	–2.412
			839.303	43279.4	162425.9	1–3	1.058–01	3.550–03	–2.450
56.	$5s^2 5p^4 - 5s^2 5p^3 5d$	${}^1S - {}^3P^\circ$	745.506	43279.4	177416.4	1–9	1.022–02	7.694–04	–3.114
			780.213	43279.4	171449.5	1–3	2.675–02	7.352–04	–3.134
57.	$5s^2 5p^4 - 5s^2 5p^3 5d$	${}^1S - {}^3S^\circ$	734.224	43279.4	179477.8	1–3	4.378–03	1.071–04	–3.970
58.	$5s^2 5p^4 - 5s^2 5p^3 6s$	${}^1S - {}^3D^\circ$	711.479	43279.4	183831.7	1–15	4.738–02	5.461–03	–2.263
			717.907	43279.4	182573.3	1–3	2.306–01	5.412–03	–2.267

Table A5 – continued

No.	Transition Array	Mult.	λ_{vac} (Å)	E_i (cm $^{-1}$)	E_k (cm $^{-1}$)	g_i-g_k	A_{ki} (10 8 s $^{-1}$)	f_{ik}	$\log g f$
59.	$5s^25p^4 - 5s^25p^35d$	${}^1S - {}^3D^\circ$	713.212	43279.4	183490.2	1–15	5.199–02	5.614–03	–2.251
			684.405	43279.4	189391.7	1–3	2.942–01	5.850–03	–2.233
60.	$5s^25p^4 - 5s^25p^35d$	${}^1S - {}^3P^\circ$	693.635	43279.4	187447.4	1–9	1.070–01	6.741–03	–2.171
			701.093	43279.4	185913.9	1–3	3.110–01	6.669–03	–2.176
61.	$5s^25p^4 - 5s5p^5$	${}^1S - {}^1P^\circ$	660.474	43279.4	194685.9	1–3	4.228+00	8.049–02	–1.094
62.	$5s^25p^4 - 5s^25p^36s$	${}^1S - {}^3P^\circ$	623.333	43279.4	203707.3	1–9	3.182–01	1.635–02	–1.787
			644.186	43279.4	198514.1	1–3	8.650–01	1.582–02	–1.801
63.	$5s^25p^4 - 5s^25p^36s$	${}^1S - {}^1P^\circ$	605.251	43279.4	208500.0	1–3	8.131+00	1.343–01	–0.872
64.	$5s^25p^4 - 5s^25p^35d$	${}^1S - {}^1P^\circ$	589.051	43279.4	213044.0	1–3	3.050+02	4.744+00	0.676

Table A6. Cs v: List of tabulated lines ordered in increasing wavelengths for allowed transitions that are given in Table A7.

Wavelength (Å)	No.						
421.337	18	522.743	30	591.050	46	700.154	23
425.183	18	522.912	8	591.567	27	714.360	43
446.427	17	523.279	31	592.379	51	714.494	2
446.749	14	524.354	33	594.628	49	714.519	23
449.918	37	525.967	34	595.691	28	714.828	22
450.585	15	526.034	36	597.921	26	726.708	43
454.307	37	526.338	8	599.520	6	727.117	23
454.518	13	526.364	52	608.131	48	742.955	22
459.233	12	531.220	9	609.376	48	750.170	41
460.901	37	531.739	50	610.236	25	751.138	44
461.605	16	532.993	8	612.080	47	771.230	43
465.508	37	536.658	30	613.762	52	773.661	20
466.934	13	537.449	28	623.055	22	785.643	43
472.867	12	537.628	30	623.722	5	791.780	40
473.744	14	540.406	31	623.723	25	793.954	42
478.645	36	541.464	53	627.803	45	794.544	1
479.014	33	542.517	29	629.454	46	800.757	20
483.427	34	548.811	50	631.916	3	803.042	43
483.765	11	550.276	54	632.747	45	806.715	20
484.553	11	550.765	51	633.300	5	811.738	1
486.881	55	554.782	29	633.513	49	812.876	41
487.322	15	556.606	52	636.417	47	836.220	20
487.958	32	557.026	49	637.514	24	847.069	42
491.094	36	558.566	29	639.817	46	862.254	40
491.483	33	562.621	50	645.030	25	864.832	42
493.395	31	567.668	26	645.281	4	877.950	1
496.129	34	569.551	4	647.331	24	887.331	41
496.135	35	569.862	49	653.361	47	902.683	19
497.162	9	570.109	7	659.097	24	924.940	19
499.691	12	571.576	29	659.791	24	925.857	39
501.496	10	571.707	26	665.056	24	972.584	19
502.296	32	573.313	48	671.307	45	979.822	39
506.634	31	573.520	53	676.964	45	1011.896	19
509.168	31	577.194	52	680.932	23	1023.693	39
510.186	33	577.472	28	682.936	24	1064.881	38
511.958	10	579.568	26	685.062	46	1069.196	19
512.646	55	581.610	6	688.013	45	1095.995	38
516.023	32	581.769	50	688.466	23	1196.392	38
518.352	55	589.558	26	692.842	2	1235.807	38
521.136	51	589.769	6	696.254	41	1396.102	38
521.826	30	591.008	49	698.463	21		

Table A7. Cs v: Allowed transitions (values of A_{ki} and f_{ik} are given with the notation $a \pm b \equiv a \times 10^{\pm b}$).

No.	Transition Array	Mult.	λ_{vac} (Å)	E_i (cm $^{-1}$)	E_k (cm $^{-1}$)	$g_i - g_k$	A_{ki} (10 8 s $^{-1}$)	f_{ik}	$\log g f$
1.	$5s^2 5p^3 - 5s 5p^4$	${}^4S^\circ - {}^4P$	840.397	0.0	118991.4	4–12	4.292+00	1.361–01	–0.264
			877.950	0.0	113901.7	4–6	3.382+00	5.855–02	–0.630
			811.738	0.0	123192.4	4–4	5.165+00	5.075–02	–0.693
			794.544	0.0	125858.3	4–2	5.766+00	2.737–02	–0.961
2.	$5s^2 5p^3 - 5s 5p^4$	${}^4S^\circ - {}^2D$	701.343	0.0	142583.5	4–10	3.111–01	5.727–03	–1.640
			714.494	0.0	139959.2	4–4	5.272–01	4.025–03	–1.793
			692.842	0.0	144333.0	4–6	1.524–01	1.646–03	–2.182
3.	$5s^2 5p^3 - 5s 5p^4$	${}^4S^\circ - {}^2S$	631.916	0.0	158248.8	4–2	2.916+00	8.938–03	–1.447
4.	$5s^2 5p^3 - 5s^2 5p^2 5d$	${}^4S^\circ - {}^2P$	617.894	0.0	161839.8	4–6	7.638–01	6.633–03	–1.576
			645.281	0.0	154971.2	4–4	6.312–01	3.937–03	–1.803
			569.551	0.0	175576.8	4–2	1.090+00	2.735–03	–1.961
5.	$5s^2 5p^3 - 5s^2 5p^2 5d$	${}^4S^\circ - {}^4F$	601.039	0.0	166378.5	4–28	1.684+00	6.388–02	–0.593
			633.300	0.0	157903.0	4–4	1.872+00	1.123–02	–1.348
			623.722	0.0	160327.9	4–6	5.725+00	5.015–02	–0.698
6.	$5s^2 5p^3 - 5s^2 5p^2 5d$	${}^4S^\circ - {}^4D$	589.352	0.0	169677.8	4–20	2.758+00	7.165–02	–0.543
			589.769	0.0	169557.9	4–2	2.249–02	6.140–05	–3.610
			599.520	0.0	166800.2	4–6	5.817+00	4.607–02	–0.734
			581.610	0.0	171936.7	4–4	4.778+00	2.505–02	–0.999
7.	$5s^2 5p^3 - 5s^2 5p^2 5d$	${}^4S^\circ - {}^2F$	554.150	0.0	180456.1	4–14	1.447+00	2.316–02	–1.033
			570.109	0.0	175405.0	4–6	3.100+00	2.251–02	–1.046
8.	$5s^2 5p^3 - 5s^2 5p^2 5d$	${}^4S^\circ - {}^4P$	529.063	0.0	189013.4	4–12	2.557+02	3.167+00	1.103
			532.993	0.0	187619.8	4–6	2.826+02	1.779+00	0.852
			526.338	0.0	189992.1	4–4	1.788+02	7.267–01	0.463
			522.912	0.0	191236.7	4–2	3.263+02	6.590–01	0.421
9.	$5s^2 5p^3 - 5s 5p^4$	${}^4S^\circ - {}^2P$	519.361	0.0	192544.4	4–6	1.026+02	6.043–01	0.383
			531.220	0.0	188245.8	4–4	1.425+02	5.852–01	0.369
			497.162	0.0	201141.6	4–2	3.277+00	5.980–03	-1.621
10.	$5s^2 5p^3 - 5s^2 5p^2 5d$	${}^4S^\circ - {}^2D$	505.629	0.0	197773.5	4–10	3.287+01	3.028–01	0.083
			511.958	0.0	195328.4	4–4	2.509+01	9.690–02	–0.412
			501.496	0.0	199403.5	4–6	3.836+01	2.064–01	–0.083
11.	$5s^2 5p^3 - 5s^2 5p^2 5d$	${}^4S^\circ - {}^2D$	484.080	0.0	206577.6	4–10	1.068+00	9.188–03	–1.435
			484.553	0.0	206375.9	4–4	2.657+00	9.165–03	–1.436
			483.765	0.0	206712.0	4–6	2.716–03	1.386–05	–4.256
12.	$5s^2 5p^3 - 5s^2 5p^2 6s$	${}^4S^\circ - {}^4P$	470.094	0.0	212723.2	4–12	2.896+01	2.899–01	0.064
			499.691	0.0	200123.6	4–2	3.224+01	5.978–02	–0.621
			472.867	0.0	211476.1	4–4	2.538+01	8.632–02	–0.462
			459.233	0.0	217754.6	4–6	2.980+01	1.428–01	–0.243

Table A7 – continued

No.	Transition Array	Mult.	λ_{vac} (Å)	E_i (cm $^{-1}$)	E_k (cm $^{-1}$)	g_{i-gk}	A_{ki} (10 8 s $^{-1}$)	f_{ik}	$\log g f$
13.	$5s^25p^3 - 5s^25p^26s$	${}^4S^\circ - {}^2P$	462.721	0.0	216113.1	4–6	2.954+00	1.398–02	-1.252
			466.934	0.0	214163.1	4–4	1.393–02	4.482–05	-3.746
			454.518	0.0	220013.2	4–2	9.319+00	1.419–02	-1.246
14.	$5s^25p^3 - 5s^25p^25d$	${}^4S^\circ - {}^2D$	462.564	0.0	216186.4	4–10	4.321+00	3.466–02	-0.858
			473.744	0.0	211084.4	4–6	6.612+00	3.340–02	-0.874
			446.749	0.0	223839.4	4–4	1.640–01	4.695–04	-2.726
15.	$5s^25p^3 - 5s^25p^25d$	${}^4S^\circ - {}^2P$	462.199	0.0	216356.9	4–6	5.401+00	2.510–02	-0.998
			487.322	0.0	205203.2	4–2	1.966+00	3.422–03	-1.864
			450.585	0.0	221933.8	4–4	7.500+00	2.205–02	-1.055
16.	$5s^25p^3 - 5s^25p^25d$	${}^4S^\circ - {}^2S$	461.605	0.0	216635.5	4–2	8.199+00	1.301–02	-1.284
17.	$5s^25p^3 - 5s^25p^25d$	${}^4S^\circ - {}^2F$	453.656	0.0	220431.5	4–14	1.966+00	2.043–02	-1.088
			446.427	0.0	224000.6	4–6	4.813+00	2.076–02	-1.081
18.	$5s^25p^3 - 5s^25p^26s$	${}^4S^\circ - {}^2D$	423.636	0.0	236051.7	4–10	1.655+00	1.108–02	-1.353
			425.183	0.0	235192.8	4–6	2.208+00	8.875–03	-1.450
			421.337	0.0	237340.0	4–4	8.276–01	2.186–03	-2.058
19.	$5s^25p^3 - 5s5p^4$	${}^2D^\circ - {}^4P$	992.691	18255.1	118991.4	10–12	6.496–01	1.149–02	-0.940
			1011.896	15077.4	113901.7	4–6	6.080–01	1.396–02	-1.253
			924.940	15077.4	123192.4	4–4	1.122–02	1.429–04	-3.243
			902.683	15077.4	125858.3	4–2	7.517–02	4.605–04	-2.735
			1069.196	20373.5	113901.7	6–6	3.628–01	6.212–03	-1.429
			972.584	20373.5	123192.4	6–4	2.824–01	2.653–03	-1.798
20.	$5s^25p^3 - 5s5p^4$	${}^2D^\circ - {}^2D$	804.321	18255.1	142583.5	10–10	7.060+00	6.840–02	-0.165
			800.757	15077.4	139959.2	4–4	8.634+00	8.272–02	-0.480
			773.661	15077.4	144333.0	4–6	1.694–05	2.279–07	-6.040
			836.220	20373.5	139959.2	6–4	4.152–01	2.895–03	-1.760
			806.715	20373.5	144333.0	6–6	5.724+00	5.592–02	-0.474
21.	$5s^25p^3 - 5s5p^4$	${}^2D^\circ - {}^2S$	714.318	18255.1	158248.8	10–2	1.227+01	1.925–02	-0.716
			698.463	15077.4	158248.8	4–2	1.313+01	4.923–02	-0.706
22.	$5s^25p^3 - 5s^25p^25d$	${}^2D^\circ - {}^2P$	696.453	18255.1	161839.7	10–6	5.517+00	2.419–02	-0.616
			714.828	15077.4	154971.2	4–4	4.225–01	3.230–03	-1.889
			742.955	20373.5	154971.2	6–4	5.382+00	2.968–02	-0.749
			623.055	15077.4	175576.8	4–2	3.591+00	1.081–02	-1.364
23.	$5s^25p^3 - 5s^25p^25d$	${}^2D^\circ - {}^4F$	675.113	18255.1	166378.5	10–28	1.175+00	2.245–02	-0.649
			700.154	15077.4	157903.0	4–4	1.497+00	1.097–02	-1.358
			727.117	20373.5	157903.0	6–4	4.147+00	2.187–02	-0.882
			688.466	15077.4	160327.9	4–6	1.954–01	2.084–03	-2.079
			714.519	20373.5	160327.9	6–6	2.309–01	1.772–03	-1.973
			680.932	20373.5	167231.1	6–8	3.169–01	2.968–03	-1.749

Table A7 – continued

No.	Transition Array	Mult.	λ_{vac} (Å)	E_i (cm $^{-1}$)	E_k (cm $^{-1}$)	$g_i - g_k$	A_{ik} (10 8 s $^{-1}$)	f_{ik}	$\log g f$
24.	$5s^2 5p^3 - 5s^2 5p^2 5d$	$^2D^\circ - ^4D$	660.403	18255.1	169677.8	10–20	2.443+00	3.271–02	−0.485
			647.331	15077.4	169557.9	4–2	3.354+00	1.108–02	−1.354
			659.097	15077.4	166800.2	4–6	3.225–01	3.080–03	−1.909
			682.936	20373.5	166800.2	6–6	9.962–01	6.810–03	−1.389
			637.514	15077.4	171936.7	4–4	2.002+00	1.264–02	−1.296
			659.791	20373.5	171936.7	6–4	5.138+00	2.322–02	−0.856
			665.056	20373.5	170736.7	6–8	7.734–01	6.808–03	−1.389
25.	$5s^2 5p^3 - 5s^2 5p^2 5d$	$^2D^\circ - ^2F$	616.519	18255.1	180456.1	10–14	5.557+00	4.417–02	−0.355
			623.723	15077.4	175405.0	4–6	3.255+00	2.825–02	−0.947
			645.030	20373.5	175405.0	6–6	2.714+00	1.682–02	−0.996
			610.236	20373.5	184244.5	6–8	5.017+00	3.735–02	−0.650
26.	$5s^2 5p^3 - 5s^2 5p^2 5d$	$^2D^\circ - ^4P$	585.623	18255.1	189013.4	10–12	5.078+01	3.067–01	0.487
			579.568	15077.4	187619.8	4–6	2.131+01	1.583–01	−0.198
			597.921	20373.5	187619.8	6–6	1.069+01	5.640–02	−0.471
			571.707	15077.4	189992.1	4–4	5.065+01	2.423–01	−0.014
			589.558	20373.5	189992.1	6–4	5.506+01	1.868–01	0.050
			567.668	15077.4	191236.7	4–2	2.173+00	5.163–03	−1.685
27.	$5s^2 5p^3 - 5s^2 5p^2 5d$	$^2D^\circ - ^2G$	577.757	18255.1	191338.3	10–18	4.003+00	3.549–02	−0.450
			591.567	20373.5	189415.9	6–8	8.391+00	5.777–02	−0.460
28.	$5s^2 5p^3 - 5s 5p^4$	$^2D^\circ - ^2P$	573.758	18255.1	192544.4	10–6	1.569+02	4.524–01	0.655
			577.472	15077.4	188245.8	4–4	5.240+01	2.535–01	0.006
			595.691	20373.5	188245.8	6–4	8.364+01	2.870–01	0.236
			537.449	15077.4	201141.6	4–2	2.151+02	4.578–01	0.263
29.	$5s^2 5p^3 - 5s^2 5p^2 5d$	$^2D^\circ - ^2D$	557.046	18255.1	197773.5	10–10	1.475+02	6.508–01	0.813
			554.782	15077.4	195328.4	4–4	3.298–02	1.493–04	−3.224
			571.576	20373.5	195328.4	6–4	1.474+01	4.723–02	−0.548
			542.517	15077.4	199403.5	4–6	1.555+02	9.748–01	0.591
			558.566	20373.5	199403.5	6–6	9.086+01	4.022–01	0.383
30.	$5s^2 5p^3 - 5s^2 5p^2 5d$	$^2D^\circ - ^2D$	531.004	18255.1	206577.6	10–10	2.246+02	9.219–01	0.965
			522.743	15077.4	206375.9	4–4	2.002+02	8.020–01	0.506
			537.628	20373.5	206375.9	6–4	2.995+01	8.462–02	−0.294
			521.826	15077.4	206712.0	4–6	5.738+01	3.397–01	0.133
			536.658	20373.5	206712.0	6–6	1.664+02	6.945–01	0.620
31.	$5s^2 5p^3 - 5s^2 5p^2 6s$	$^2D^\circ - ^4P$	514.223	18255.1	212723.2	10–12	2.725+01	1.316–01	0.119
			540.406	15077.4	200123.6	4–2	1.080+00	2.338–03	−2.029
			509.168	15077.4	211476.1	4–4	3.254+01	1.284–01	−0.289
			523.279	20373.5	211476.1	6–4	4.389+01	1.221–01	−0.135
			493.395	15077.4	217754.6	4–6	1.334–04	7.380–07	−5.530
			506.634	20373.5	217754.6	6–6	2.283+00	8.890–03	−1.273
32.	$5s^2 5p^3 - 5s^2 5p^2 6s$	$^2D^\circ - ^2P$	505.413	18255.1	216113.2	10–6	1.055+02	1.531–01	0.185
			502.296	15077.4	214163.1	4–4	6.396+00	2.377–02	−1.022
			516.023	20373.5	214163.1	6–4	4.717+01	1.234–01	−0.131
			487.958	15077.4	220013.2	4–2	1.005+02	1.761–01	−0.152

Table A7 – continued

No.	Transition Array	Mult.	λ_{vac} (Å)	E_i (cm $^{-1}$)	E_k (cm $^{-1}$)	g_i-g_k	A_{ki} (10 8 s $^{-1}$)	f_{ik}	$\log g f$
33.	$5s^25p^3 - 5s^25p^25d$	${}^2D^\circ - {}^2D$	505.226	18255.1	216186.4	10–10	1.130+02	4.323–01	0.636
			510.186	15077.4	211084.4	4–6	1.318+02	7.717–01	0.490
			524.354	20373.5	211084.4	6–6	4.408+01	1.820–01	0.038
			479.014	15077.4	223838.4	4–4	1.444–01	4.732–04	-2.723
			491.483	20373.5	223838.4	6–4	5.217+00	1.200–02	-1.143
34.	$5s^25p^3 - 5s^25p^25d$	${}^2D^\circ - {}^2P$	504.791	18255.1	216357.0	10–6	3.212+01	7.105–02	-0.148
			525.967	15077.4	205203.2	4–2	1.238+01	2.505–02	-0.999
			483.427	15077.4	221933.8	4–4	1.322+01	4.463–02	-0.748
			496.129	20373.5	221933.8	6–4	3.115+01	7.378–02	-0.354
35.	$5s^25p^3 - 5s^25p^25d$	${}^2D^\circ - {}^2S$	504.082	18255.1	216635.5	10–2	1.923+01	1.455–02	-0.837
			496.135	15077.4	216635.5	4–2	2.017+01	3.695–02	-0.830
36.	$5s^25p^3 - 5s^25p^25d$	${}^2D^\circ - {}^2F$	505.008	18255.1	216271.9	10–14	2.502+02	1.292+00	1.111
			526.034	20373.5	210475.3	6–8	3.851+02	2.055+00	1.091
			478.645	15077.4	224000.6	4–6	2.419+00	1.196–02	-1.320
			491.094	20373.5	224000.6	6–6	1.555+00	5.390–03	-1.490
37.	$5s^25p^3 - 5s^25p^26s$	${}^2D^\circ - {}^2D$	459.144	18255.1	236051.7	10–10	4.107+01	1.283–01	0.108
			454.307	15077.4	235192.8	4–6	1.795+01	8.227–02	-0.483
			449.918	15077.4	237340.0	4–4	4.655+00	1.401–02	-1.252
			465.508	20373.5	235192.8	6–6	4.034+01	1.295–01	-0.110
			460.901	20373.5	237340.0	6–4	9.058+00	1.908–02	-0.941
38.	$5s^25p^3 - 5s5p^4$	${}^2P^\circ - {}^4P$	1247.527	38832.8	118991.4	6–12	1.155–01	5.386–03	-1.491
			1095.995	31951.1	123192.4	2–4	2.536–03	9.020–05	-3.744
			1064.881	31951.1	125858.3	2–2	5.239–01	8.905–03	-1.749
			1396.102	42273.7	113901.7	4–6	7.892–03	3.462–04	-2.859
			1235.807	42273.7	123192.4	4–4	1.137–01	2.590–03	-1.985
39.	$5s^25p^3 - 5s5p^4$	${}^2P^\circ - {}^2D$	963.849	38832.8	142583.5	6–10	9.622–01	2.237–02	-0.872
			925.857	31951.1	139959.2	2–4	2.831–01	7.225–03	-1.840
			1023.693	42273.7	139959.2	4–4	6.095–02	9.567–04	-2.417
40.	$5s^25p^3 - 5s5p^4$	${}^2P^\circ - {}^2S$	979.822	42273.7	144333.0	4–6	1.321+00	2.860–02	-0.942
			791.780	31951.1	158248.8	2–2	5.676+00	5.475–02	-0.961
			862.254	42273.7	158248.8	4–2	7.006–05	4.040–07	-5.792
41.	$5s^25p^3 - 5s^25p^25d$	${}^2P^\circ - {}^2P$	812.963	38832.8	161839.7	6–6	3.097+00	3.162–02	-0.722
			812.876	31951.1	154971.2	2–4	7.123–01	1.404–02	-1.552
			887.331	42273.7	154971.2	4–4	4.548–01	5.372–03	-1.668
			696.254	31951.1	175576.8	2–2	1.123+00	8.450–03	-1.772
42.	$5s^25p^3 - 5s^25p^25d$	${}^2P^\circ - {}^4F$	750.170	42273.7	175576.8	4–2	7.611+00	3.353–02	-0.873
			784.033	38832.8	166378.5	6–28	3.294–02	1.416–03	-2.071
			793.954	31951.1	157903.0	2–4	7.321–03	1.374–04	-3.561
			864.832	42273.7	157903.0	4–4	1.376–01	1.541–03	-2.210
			847.069	42273.7	160327.9	4–6	2.023–02	3.275–04	-2.883

Table A7 – continued

No.	Transition Array	Mult.	λ_{vac} (Å)	E_i (cm $^{-1}$)	E_k (cm $^{-1}$)	$g_i - g_k$	A_{ki} (10 8 s $^{-1}$)	f_{ik}	$\log g f$	
43.	$5s^2 5p^3 - 5s^2 5p^2 5d$	${}^2P^\circ - {}^4D$	764.263	38832.8	169677.8	6–20	4.110–01	1.263–02	–1.120	
				726.708	31951.1	169557.9	2–2	2.472+00	2.064–02	–1.384
				785.643	42273.7	169557.9	4–2	1.066+00	5.252–03	–1.678
				803.042	42273.7	166800.2	4–6	3.655–02	5.168–04	–2.685
				714.360	31951.1	171936.7	2–4	1.991–01	3.160–03	–2.199
				771.230	42273.7	171936.7	4–4	1.822–01	1.700–03	–2.167
44.	$5s^2 5p^3 - 5s^2 5p^2 5d$	${}^2P^\circ - {}^2F$	706.098	38832.8	180456.2	6–14	3.721–02	6.447–04	–2.413	
				751.138	42273.7	175405.0	4–6	7.213–02	9.090–04	–2.439
45.	$5s^2 5p^3 - 5s^2 5p^2 5d$	${}^2P^\circ - {}^4P$	665.865	38832.8	189013.4	6–12	2.705+00	3.511–02	–0.676	
				688.013	42273.7	187619.8	4–6	4.211–01	4.407–03	–1.754
				632.747	31951.1	189992.1	2–4	6.371–01	7.430–03	–1.828
				676.964	42273.7	189992.1	4–4	4.424+00	2.960–02	–0.927
				627.803	31951.1	191236.7	2–2	2.572+00	1.488–02	–1.526
				671.307	42273.7	191236.7	4–2	2.235+00	7.415–03	–1.528
46.	$5s^2 5p^3 - 5s 5p^4$	${}^2P^\circ - {}^2P$	650.569	38832.8	192544.4	6–6	1.759+01	1.091–01	–0.184	
				639.817	31951.1	188245.8	2–4	4.799+00	5.665–02	–0.946
				685.062	42273.7	188245.8	4–4	8.608–01	5.838–03	–1.632
				591.050	31951.1	201141.6	2–2	2.759+01	1.416–01	–0.548
				629.454	42273.7	201141.6	4–2	2.313+01	6.748–02	–0.569
47.	$5s^2 5p^3 - 5s^2 5p^2 5d$	${}^2P^\circ - {}^2D$	629.165	38832.8	197773.4	6–10	8.229+00	7.855–02	–0.327	
				612.080	31951.1	195328.4	2–4	1.505+01	1.652–01	–0.481
				653.361	42273.7	195328.4	4–4	5.413–02	3.395–04	–2.867
				636.417	42273.7	199403.5	4–6	4.286+00	3.670–02	–0.833
48.	$5s^2 5p^3 - 5s^2 5p^2 5d$	${}^2P^\circ - {}^2D$	596.144	38832.8	206577.6	6–10	9.147+00	7.847–02	–0.327	
				573.313	31951.1	206375.9	2–4	6.821+00	6.545–02	–0.883
				609.376	42273.7	206375.9	4–4	6.240–04	3.392–06	–4.867
				608.131	42273.7	206712.0	4–6	1.055+01	8.452–02	–0.471
49.	$5s^2 5p^3 - 5s^2 5p^2 6s$	${}^2P^\circ - {}^4P$	575.075	38832.8	212723.2	6–12	4.727+00	4.711–02	–0.549	
				594.628	31951.1	200123.6	2–2	9.489+00	4.959–02	–1.004
				557.026	31951.1	211476.1	2–4	5.280+00	4.984–02	–1.001
				633.513	42273.7	200123.6	4–2	7.718–02	2.297–04	–3.037
				591.008	42273.7	211476.1	4–4	3.029+00	1.618–02	–1.189
50.	$5s^2 5p^3 - 5s^2 5p^2 6s$	${}^2P^\circ - {}^2P$	564.078	38832.8	216113.2	6–6	1.148+02	5.370–01	0.508	
				548.811	31951.1	214163.1	2–4	1.447+01	1.280–01	–0.592
				581.769	42273.7	214163.1	4–4	4.015+01	2.000–01	–0.097
				531.739	31951.1	220013.2	2–2	6.937+01	2.876–01	–0.240
				562.621	42273.7	220013.2	4–2	1.730+02	4.025–01	0.207
51.	$5s^2 5p^3 - 5s^2 5p^2 5d$	${}^2P^\circ - {}^2D$	563.845	38832.8	216186.4	6–10	1.010+02	7.603–01	0.659	
				521.136	31951.1	223839.4	2–4	2.899+02	2.237+00	0.651
				592.379	42273.7	211084.4	4–6	8.327–01	6.590–03	–1.579
				550.765	42273.7	223839.4	4–4	2.367+01	1.021–01	–0.389

Table A7 – continued

No.	Transition Array	Mult.	λ_{vac} (Å)	E_i (cm $^{-1}$)	E_k (cm $^{-1}$)	$g_i - g_k$	A_{ki} (10 8 s $^{-1}$)	f_{ik}	$\log g f$
52.	$5s^2 5p^3 - 5s^2 5p^2 5d$	$2P^\circ - 2P$	563.304	38832.8	216356.9	6–6	1.358+02	6.209–01	0.571
			577.194	31951.1	205203.2	2–2	6.991+01	3.391–01	–0.169
			613.762	42273.7	205203.2	4–2	3.168+00	8.710–03	–1.458
			526.364	31951.1	221933.8	2–4	5.556+01	4.422–01	–0.053
			556.606	42273.7	221933.8	4–4	1.230+02	5.480–01	0.341
53.	$5s^2 5p^3 - 5s^2 5p^2 5d$	$2P^\circ - 2S$	562.421	38832.8	216635.5	6–2	2.152+02	3.373–01	0.306
			541.464	31951.1	216635.5	2–2	1.266+02	5.510–01	0.042
			573.520	42273.7	216635.5	4–2	9.638+01	2.361–01	–0.025
54.	$5s^2 5p^3 - 5s^2 5p^2 5d$	$2P^\circ - 2F$	550.665	38832.8	220431.4	6–14	1.182+02	1.197+00	0.856
			550.276	42273.7	224000.6	4–6	2.764+02	1.798+00	0.857
55.	$5s^2 5p^3 - 5s^2 5p^2 6s$	$2P^\circ - 2D$	507.051	38832.8	236051.7	6–10	1.166+02	7.420–01	0.649
			486.881	31951.1	237340.0	2–4	1.211+01	8.520–02	–0.769
			518.352	42273.7	235192.8	4–6	7.165+01	4.275–01	0.233
			512.646	42273.7	237340.0	4–4	1.608+02	6.285–01	0.400

Table A8. Cs vr: List of tabulated lines ordered in increasing wavelengths for allowed transitions that are given in Table A9.

Wavelength (Å)	No.						
378.463	14	500.504	10	572.299	23	729.141	3
396.746	14	504.097	10	589.477	6	732.225	3
401.968	13	506.024	9	589.695	6	748.118	18
405.517	14	507.734	26	607.027	24	758.917	2
410.308	13	508.756	8	609.284	6	811.458	31
410.975	13	514.090	10	611.736	5	827.038	2
431.007	12	514.242	7	615.316	22	830.464	2
431.885	13	520.381	9	618.140	33	835.321	17
434.712	13	522.297	25	627.354	21	836.185	2
436.366	28	522.715	36	632.843	5	839.371	17
442.300	13	532.985	10	638.756	4	866.092	2
442.692	27	539.364	8	648.516	3	876.128	2
454.879	12	548.592	7	656.993	20	971.049	16
466.447	12	548.937	10	661.804	4	982.436	30
466.884	8	552.665	24	678.480	34	1020.117	16
472.107	37	555.706	8	681.692	20	1034.069	16
478.709	11	556.779	35	701.263	3	1055.938	1
479.254	27	558.271	22	703.974	32	1120.444	1
490.613	10	564.700	24	704.116	3	1260.137	29
495.025	8	565.506	7	711.319	19	1392.425	15
498.127	8	569.329	5	711.953	3		

Table A9. Cs vr: Allowed transitions (values of A_{ki} and f_{ik} are given with the notation $a \pm b \equiv a \times 10^{\pm b}$).

No.	Transition Array	Mult.	λ_{vac} (Å)	E_i (cm $^{-1}$)	E_k (cm $^{-1}$)	$g_i - g_k$	A_{ki} (10 8 s $^{-1}$)	f_{ik}	$\log g f$
1.	$5s^2 5p^2 - 5s 5p^3$	${}^3P - {}^5S^\circ$	1074.963	13852.1	106878.6	9–5	5.609–01	5.383–03	−1.315
			1055.938	12176.0	106878.6	3–5	2.878–01	7.980–03	−1.621
			1120.444	17628.2	106878.6	5–5	2.544–01	4.784–03	−1.621
2.	$5s^2 5p^2 - 5s 5p^3$	${}^3P - {}^3D^\circ$	824.508	13852.1	135136.5	9–15	4.920+00	8.321–02	−0.126
			758.917	0.0	131766.8	1–3	8.935+00	2.297–01	−0.639
			836.185	12176.0	131766.8	3–3	2.732–02	2.857–04	−3.067
			876.128	17628.2	131766.8	5–3	8.390–01	5.796–03	−1.538
			827.038	12176.0	133089.4	3–5	5.617+00	9.563–02	−0.542
			866.092	17628.2	133089.4	5–5	1.011–01	1.136–03	−2.246
3.	$5s^2 5p^2 - 5s 5p^3$	${}^3P - {}^3P^\circ$	711.778	13852.1	154345.4	9–9	1.649+01	1.250–01	0.051
			711.953	12176.0	152634.7	3–1	1.649+01	4.180–02	−0.902
			648.516	0.0	154198.2	1–3	5.904+00	1.112–01	−0.954
			704.116	12176.0	154198.2	3–3	1.500+01	1.116–01	−0.475
			732.225	17628.2	154198.2	5–3	4.730–01	2.290–03	−1.941
			701.263	12176.0	154775.8	3–5	9.163–02	1.118–03	−2.474
			729.141	17628.2	154775.8	5–5	1.358+01	1.077–01	−0.269
4.	$5s^2 5p^2 - 5s^2 5p 5d$	${}^3P - {}^1D^\circ$	645.669	13852.1	168730.2	9–5	9.973–01	3.445–03	−1.509
			638.756	12176.0	168730.2	3–5	1.015+00	1.029–02	−1.510
			661.804	17628.2	168730.2	5–5	1.353–02	8.858–05	−3.354
5.	$5s^2 5p^2 - 5s 5p^3$	${}^3P - {}^3S^\circ$	618.073	13852.1	175645.3	9–3	1.984+02	3.771–01	0.531
			569.329	0.0	175645.3	1–3	2.889+01	4.173–01	−0.380
			611.736	12176.0	175645.3	3–3	4.834+01	2.697–01	−0.092
6.	$5s^2 5p^2 - 5s^2 5p 5d$	${}^3P - {}^3F^\circ$	564.665	13852.1	190948.3	9–21	1.019+01	1.132–01	0.008
			589.695	12176.0	181755.2	3–5	4.610+00	3.973–02	−0.924
			609.284	17628.2	181755.2	5–5	8.442+00	4.670–02	−0.632
			589.477	17628.2	187270.0	5–7	1.692+01	1.230–01	−0.211
7.	$5s^2 5p^2 - 5s 5p^3$	${}^3P - {}^1P^\circ$	553.683	13852.1	194461.0	9–3	5.473+01	8.350–02	−0.124
			514.242	0.0	194461.0	1–3	2.989+01	3.533–01	−0.452
			548.592	12176.0	194461.0	3–3	3.003+01	1.351–01	−0.392
8.	$5s^2 5p^2 - 5s^2 5p 5d$	${}^3P - {}^3P^\circ$	565.506	17628.2	194461.0	5–3	1.480+00	4.254–03	−1.672
			539.364	12176.0	197579.4	3–5	1.138+02	8.260–01	0.394
			555.706	17628.2	197579.4	5–5	9.018+01	4.180–01	0.320
			498.127	12176.0	212928.1	3–1	2.325+02	2.904–01	−0.060
			466.884	0.0	214185.9	1–3	5.683–01	5.552–03	−2.256
			495.025	12176.0	214185.9	3–3	1.477+02	5.427–01	0.212
9.	$5s^2 5p^2 - 5s 5p^3$	${}^3P - {}^1D^\circ$	508.756	17628.2	214185.9	5–3	6.308+01	1.471–01	−0.133
			510.352	13852.1	209795.3	9–5	2.150+02	4.709–01	0.627
			506.024	12176.0	209795.3	3–5	1.388+02	8.960–01	0.429
			520.381	17628.2	209795.3	5–5	7.520+01	3.086–01	0.188

Table A9 – continued

No.	Transition Array	Mult.	λ_{vac} (Å)	E_i (cm $^{-1}$)	E_k (cm $^{-1}$)	$g_i - g_k$	A_{ki} (10 8 s $^{-1}$)	f_{ik}	$\log g f$
10.	$5s^2 5p^2 - 5s^2 5p5d$	${}^3P - {}^3D^\circ$	507.330	13852.1	210962.4	9–15	2.298+02	1.462+00	1.119
			500.504	0.0	199798.6	1–3	2.379+02	2.631+00	0.420
			532.985	12176.0	199798.6	3–3	5.529+01	2.318–01	–0.158
			548.937	17628.2	199798.6	5–3	4.886+00	1.305–02	–1.185
			514.090	17628.2	212146.6	5–7	2.754+02	1.512+00	0.879
			490.613	12176.0	216002.8	3–5	3.421+01	2.054–01	–0.210
			504.097	17628.2	216002.8	5–5	7.951+01	3.030–01	0.180
11.	$5s^2 5p^2 - 5s^2 5p5d$	${}^3P - {}^1F^\circ$	470.209	13852.1	226523.4	9–7	4.527+01	1.166–01	0.021
			478.709	17628.2	226523.4	5–7	4.290+01	2.062–01	0.013
12.	$5s^2 5p^2 - 5s^2 5p5d$	${}^3P - {}^1P^\circ$	458.373	13852.1	232014.9	9–3	9.958+00	1.044–02	–1.027
			431.007	0.0	232014.9	1–3	3.670–01	3.049–03	–2.516
			454.879	12176.0	232014.9	3–3	1.220+00	3.777–03	–1.946
			466.447	17628.2	232014.9	5–3	8.029+00	1.570–02	–1.105
13.	$5s^2 5p^2 - 5s^2 5p6s$	${}^3P - {}^3P^\circ$	417.932	13852.1	253125.7	9–9	8.681+01	2.262–01	0.309
			434.712	12176.0	242213.3	3–1	9.279+01	8.697–02	–0.584
			410.308	0.0	243719.2	1–3	3.648+01	2.717–01	–0.566
			431.885	12176.0	243719.2	3–3	2.090+01	5.763–02	–0.762
			442.300	17628.2	243719.2	5–3	5.716+01	9.932–02	–0.304
			401.968	12176.0	260952.0	3–5	2.245+01	9.117–02	–0.563
			410.975	17628.2	260952.0	5–5	4.227+01	1.078–01	–0.268
14.	$5s^2 5p^2 - 5s^2 5p6s$	${}^3P - {}^1P^\circ$	399.402	13852.1	264226.7	9–3	2.442+01	1.944–02	–0.757
			378.463	0.0	264226.7	1–3	2.569–01	1.646–03	–2.784
			396.746	12176.0	264226.7	3–3	3.221+00	7.580–03	–1.643
			405.517	17628.2	264226.7	5–3	2.011+01	2.970–02	–0.828
15.	$5s^2 5p^2 - 5s5p^3$	${}^1D - {}^5S^\circ$	1392.425	35061.4	106878.6	5–5	1.947–02	5.728–04	–2.543
16.	$5s^2 5p^2 - 5s5p^3$	${}^1D - {}^3D^\circ$	999.250	35061.4	135136.5	5–15	7.086–01	3.204–02	–0.795
			1034.069	35061.4	131766.8	5–3	4.953–01	4.814–03	–1.619
			1020.117	35061.4	133089.4	5–5	5.703–02	8.974–04	–2.348
17.	$5s^2 5p^2 - 5s5p^3$	${}^1D - {}^3P^\circ$	971.049	35061.4	138042.8	5–7	1.351+00	2.690–02	–0.871
			838.335	35061.4	154345.4	5–9	2.207–01	4.196–03	–1.678
			839.371	35061.4	154198.2	5–3	1.541–04	9.884–07	–5.306
			835.321	35061.4	154775.8	5–5	4.014–01	4.210–03	–1.677
18.	$5s^2 5p^2 - 5s^2 5p5d$	${}^1D - {}^1D^\circ$	748.118	35061.4	168730.2	5–5	8.656+00	7.288–02	–0.438
19.	$5s^2 5p^2 - 5s5p^3$	${}^1D - {}^3S^\circ$	711.319	35061.4	175645.3	5–3	4.652–01	2.124–03	–1.974
20.	$5s^2 5p^2 - 5s^2 5p5d$	${}^1D - {}^3F^\circ$	641.492	35061.4	190948.3	5–21	1.549+00	4.013–02	–0.698
			681.692	35061.4	181755.2	5–5	5.416+00	3.772–02	–0.724
			656.993	35061.4	187270.0	5–7	4.661–03	4.232–05	–3.674
21.	$5s^2 5p^2 - 5s5p^3$	${}^1D - {}^1P^\circ$	627.354	35061.4	194461.0	5–3	8.844+01	3.148–01	0.197

Table A9 – continued

No.	Transition Array	Mult.	λ_{vac} (Å)	E_i (cm $^{-1}$)	E_k (cm $^{-1}$)	$g_i - g_k$	A_{ki} (10 8 s $^{-1}$)	f_{ik}	$\log g f$
22.	$5s^2 5p^2 - 5s^2 5p5d$	${}^1D - {}^3P^\circ$	589.071	35061.4	204820.3	5–9	2.753+01	2.596–01	0.113
			615.316	35061.4	197579.4	5–5	2.202+01	1.259–01	–0.201
			558.271	35061.4	214185.9	5–3	4.788+01	1.352–01	–0.170
23.	$5s^2 5p^2 - 5s5p^3$	${}^1D - {}^1D^\circ$	572.299	35061.4	209795.3	5–5	6.031+01	3.013–01	0.178
24.	$5s^2 5p^2 - 5s^2 5p5d$	${}^1D - {}^3D^\circ$	568.502	35061.4	210962.4	5–15	6.210+01	9.048–01	0.656
			607.027	35061.4	199798.6	5–3	1.572+01	5.158–02	–0.589
			564.700	35061.4	212146.6	5–7	2.884+01	1.919–01	–0.018
			552.665	35061.4	216002.8	5–5	1.472+02	6.780–01	0.530
25.	$5s^2 5p^2 - 5s^2 5p5d$	${}^1D - {}^1F^\circ$	522.297	35061.4	226523.4	5–7	2.794+02	1.609E+00	0.905
26.	$5s^2 5p^2 - 5s^2 5p5d$	${}^1D - {}^1P^\circ$	507.734	35061.4	232014.9	5–3	1.225+01	2.851–02	–0.846
27.	$5s^2 5p^2 - 5s^2 5p6s$	${}^1D - {}^3P^\circ$	458.580	35061.4	253125.7	5–9	1.349+01	7.748–02	–0.412
			479.254	35061.4	243719.2	5–3	2.713–01	5.554–04	–2.556
			442.692	35061.4	260952.0	5–5	2.679+01	7.966–02	–0.400
28.	$5s^2 5p^2 - 5s^2 5p6s$	${}^1D - {}^1P^\circ$	436.366	35061.4	264226.7	5–3	1.109+02	1.906–01	–0.021
29.	$5s^2 5p^2 - 5s^2 5p^3$	${}^1S - {}^3D^\circ$	1208.807	52410.3	135136.5	1–15	3.666–03	1.212–03	–2.916
			1260.137	52410.3	131766.8	1–3	1.618–02	1.163–03	–2.934
30.	$5s^2 5p^2 - 5s^2 5p^3$	${}^1S - {}^3P^\circ$	981.016	52410.3	154345.4	1–9	1.379–01	1.806–02	–1.743
			982.436	52410.3	154198.2	1–3	4.118–01	1.803–02	–1.744
31.	$5s^2 5p^2 - 5s^2 5p^3$	${}^1S - {}^3S^\circ$	811.458	52410.3	175645.3	1–3	1.215+00	3.596–02	–1.444
32.	$5s^2 5p^2 - 5s^2 5p^3$	${}^1S - {}^1P^\circ$	703.974	52410.3	194461.0	1–3	9.254+00	2.067–01	–0.685
33.	$5s^2 5p^2 - 5s^2 5p5d$	${}^1S - {}^3P^\circ$	656.125	52410.3	204820.3	1–9	5.279–04	3.081–05	–4.511
			618.140	52410.3	214185.9	1–3	1.894–03	3.270–05	–4.485
34.	$5s^2 5p^2 - 5s^2 5p5d$	${}^1S - {}^3D^\circ$	630.708	52410.3	210962.4	1–15	4.462–03	3.932–04	–3.405
			678.480	52410.3	199798.6	1–3	1.792–02	3.655–04	–3.437
35.	$5s^2 5p^2 - 5s^2 5p5d$	${}^1S - {}^1P^\circ$	556.779	52410.3	232014.9	1–3	1.769+02	2.469+00	0.393
36.	$5s^2 5p^2 - 5s^2 5p6s$	${}^1S - {}^3P^\circ$	498.218	52410.3	253125.7	1–9	8.958+00	2.962–01	–0.528
			522.715	52410.3	243719.2	1–3	2.327+01	2.823–01	–0.549
37.	$5s^2 5p^2 - 5s^2 5p6s$	${}^1S - {}^1P^\circ$	472.107	52410.3	264226.7	1–3	9.001+01	9.025–01	–0.045